Energy Conversion and Management 233 (2021) 113922

Contents lists available at ScienceDirect

Energy Conversion and Management

journal homepage: www.elsevier.com/locate/enconman

# Design and thermodynamic analysis of a novel methanol, hydrogen, and power trigeneration system based on renewable energy and flue gas carbon dioxide

Reza Nazerifard [a], Leyla Khani [a], Mousa Mohammadpourfard [a,*], Behnam Mohammadi-Ivatloo [b], Gülden Gökçen Akkurt [c]

[a] Faculty of Chemical and Petroleum Engineering, University of Tabriz, Tabriz, Iran
[b] Faculty of Electrical and Computer Engineering, University of Tabriz, Tabriz, Iran
[c] Department of Energy Systems Engineering, Izmir Institute of Technology, Izmir, Turkey

ARTICLE INFO

*Keywords:*
Flue gas
Carbon dioxide
Methanol
Electrolysis
Direct methanol fuel cell
Organic Rankine cycle

ABSTRACT

In this paper, a new trigeneration system is proposed to decrease atmospheric carbon dioxide emission and produce methanol, hydrogen, and power. The system is composed of an organic Rankine cycle, a direct methanol fuel cell, a carbon capture unit, a proton exchange membrane electrolyzer, and a methanol synthesis unit. A flue gas stream with a defined composition, solar energy, and the atmospheric air are the system's inlets. In the design step, special attention is paid to heat and mass integration between different components so that its waste can be lowered as much as possible. Then, mass balance law, energy conservation principle, exergy relations, and auxiliary equations are applied for each subsystem to investigate the system's thermodynamic performance. Also, the effect of changing operating parameters on the performance of each subsystem is studied. The obtained results show that the proposed system has the energy and exergy efficiencies of 66.84% and 55.10%, respectively. Furthermore, 94% of the total exergy destruction rate belongs to the water electrolyzer, while the contribution of the organic Rankine cycle is negligible. The performance of the methanol synthesis reactor depends strongly on its inlet temperature. Maximum equilibrium methanol concentration and carbon dioxide conversion are achieved at the inlet temperature of 210 °C. The parametric studies reveal that there is an optimum fuel cell current density in which its produced power density is maximized.

## 1. Introduction

The increase in world population, economic development, human welfare demands, and production rate has led to a rise in global energy consumption, mainly supplied by fossil fuel resources. It is estimated that fossil fuels provide nearly 85% of worldwide energy needs [1]. However, the combustion of fossil fuels in power plants produces a large amount of carbon dioxide which is a greenhouse gas (GHG) and main contributor to environmental problems such as global warming, ice melting, deforestation, floods, and climate change. It is reported that nearly 7 Gt of carbon dioxide is generated each year, and the rate is expected to increase in the coming years [2]. Therefore, it is crucial to decrease carbon dioxide emissions to the environment. Among various suggestions, carbon capture and storage (CCS) and its conversion to different products have gained particular attention. In carbon capture and utilization (CCU) process, an economic benefit through the generation of a value-added material for use in other chemical processes is achieved besides the decrease of carbon dioxide release. Various components, such as methanol ($CH_3OH$), dimethyl ether ($CH_3OCH_3$), and methane ($CH_4$), can be produced from emitted carbon dioxide [3].

Methanol is a product of a catalytic regenerative conversion reaction between carbon dioxide and hydrogen. It has several advantages like high energy density, easy storage and transportation, low toxicity, and little environmental pollution [4]. Also, it can be used as raw material for producing several essential chemicals like acid acetic ($CH_3COOH$),

*Abbreviations:* Adj, Adjust; CC, Carbon capture; DMFC, Direct methanol fuel cell; EOD, Electro-osmotic drag; HX, Heat exchanger; MEA, Mono Ethanol Amine; MOR, Methanol oxidation reaction; MSR, Methanol synthesis reactor; MSU, Methanol synthesis unit; ORC, Organic Rankine cycle; ORR, Oxygen reduction reaction; PEME, Proton exchange membrane electrolyzer; RWGS, Reverse water gas shift.

* Corresponding author.
*E-mail address:* mohammadpour@tabrizu.ac.ir (M. Mohammadpourfard).

https://doi.org/10.1016/j.enconman.2021.113922
Received 27 October 2020; Received in revised form 27 October 2020; Accepted 2 February 2021
Available online 20 February 2021

**Nomenclature**

| | |
|---|---|
| A | Kinetic constant |
| $A_{cell}$ | Cell area ($m^2$) |
| $a_{H_2O}$ | Water activity |
| B | Kinetic constant |
| C | Molar concentration ($mol/m^3$) |
| D | Diffusivity ($m^2/s$) |
| $\bar{e}$ | Standard molar exergy (J/mol) |
| $\dot{E}$ | Exergy flow rate (J/mol) |
| $E_{act}$ | Activation energy (J/mol) |
| F | Faraday number (A.s/mol) |
| $\bar{h}$ | Specific molar enthalpy (J/mol) |
| HHV | Higher heating value (J/kg) |
| I | Current (A) |
| i | Current density ($A/m^2$) |
| $i_0$ | Exchange current density ($A/m^2$) |
| $i^{ref}$ | Pre-exponential factor ($A/m^2$) |
| $I_{xover}$ | Crossover current (A) |
| $i_{xover}$ | Crossover current density ($A/m^2$) |
| k | Reaction rate constant |
| $K_{reac}$ | Reaction rate constant ($mol/m^3$) |
| $\dot{M}$ | Mass flow rate (kg/s) |
| N | Number of cells in the stack |
| n | Number of transferred electrons |
| $\dot{N}$ | Molar flow rate (mol/s) |
| $n_d$ | Drag coefficient |
| p | Pressure (Pa) |
| Q | Heat (kW) |
| R | Universal gas constant (J/mol.K) |
| r | Reaction rate ($kmol/kg_{cat}.s$) |
| $R_{cont}$ | Contact resistance (Ωm2) |
| $R_{mem}$ | Membrane resistance (Ω/m2) |
| $\bar{s}$ | Specific molar entropy (J/mol) |
| T | Temperature (K) |
| $U_{rev}$ | Cell reversible potential (V) |
| v | Overpotential (V) |
| V | Voltage (V) |
| W | Power (kW) |
| X | Conversion (%) |
| ΔG | Gibbs free energy change (J) |
| ΔH | Enthalpy change (J) |

*Greek letters*

| | |
|---|---|
| α | Charge transfer coefficient |
| δ | Thickness (m) |
| ε | Porosity |
| η | Efficiency |
| λ | Water content ($mol_{H_2O}/mol_{SO_3^{-1}}$) |
| σ | Protonic conductivity (S/m) |

*Superscripts*

| | |
|---|---|
| 0 | Standard condition |
| cons | Consumption |
| in | Inlet |
| out | Outlet |
| prod | Production |
| ref | Reference |
| tot | Total |

*Subscripts*

| | |
|---|---|
| a | Anode |
| acl | Anode catalyst layer |
| act | Activation |
| amb | Ambient |
| B | Blower |
| b | Boundary |
| c | Cathode |
| C | Compressor |
| ccl | Cathode catalyst layer |
| ch | Chemical |
| conc | Concentration |
| cont | Contact |
| cross | Crossover |
| cv | Control volume |
| des | Destruction |
| diff | Diffusion |
| eff | Effective |
| k | $k_{th}$ component |
| kin | Kinetic loss |
| mem | Membrane |
| ohm | Ohmic |
| P | Pump |
| ph | Physical |
| T | Turbine |
| th | Theoretical |
| y | Molar fraction |

formaldehyde ($CH_2O$), methyl tertiary-butyl ether (MTBE), and dimethyl ether (DME) [5]. Furthermore, it can be used as an octane number booster for gasoline, and as a valuable fuel for different fuel cells [6]. So, it is concluded that carbon to methanol conversion is an excellent solution for lowering carbon dioxide emissions from power plants. Until now, many researchers have evaluated various designs for methanol production under different operating conditions [7]. However, carbon to methanol reaction needs a large amount of hydrogen, which is not available as a free component in the surroundings. The required hydrogen can be generated from the solar-powered water-splitting reaction, which is a clean process without environmental pollution. Additionally, even if all of the produced hydrogens are not consumed in the hydrogenation of carbon dioxide, surplus hydrogen may be considered as an energy storage option of solar energy for utilization during cloudy or night times. Hydrogen can also be used in fuel cells or sold as a byproduct. Although renewable energy sources cannot replace fossil fuel power plants in the near future, their integration can compensate for the adverse effects of carbon capture and utilization systems such as power consumption and power plant efficiency deterioration.

On the other hand, fossil fuel resources are limited, and their price has an increasing trend. So, it seems crucial to design more efficient energy conversion systems that can consume a significant part of fuel's chemical energy. In this regard, combining two or more different thermodynamic systems for simultaneous production of various demands like power, cooling, heating, and others from one energy source looks reasonable. These co/tri/multi-systems enjoy advantages like fair energy usage, higher efficiency, reliability, and safety in addition to lower cost and emission rates [8].

Migrand et al. [9] studied the effect of using different waste heat sources on a methanol production system from captured carbon dioxide. They concluded that the power production efficiency of renewable sources is as high as 59%. However, fossil fuel should be used to supply nearly 3.6% of system energy demand. Boretti [10] analyzed a methanol production system from the flue gas of an oxy-fuel combustion plant and hydrogen feedstock. He concluded that methanol has a higher

conversion efficiency than gasoline. Since methanol resists knock in directly injected and turbocharged engines very well, it can be a suitable choice for high power concentration. Sayah et al. [11] designed a flue gas-based methanol production and wind energy based hydrogen generation system. Their obtained results showed that the employment of their system in Iran could lead to an increase in renewable energy integration, natural gas consumption, and emitted $CO_2$ rate. Esmaili et al. [12] investigated a solar-based hydrogen and methanol generation system. By studying the effect of varying operating parameters, they proved that sunlight intensity affects system efficiency. Leonzio et al. [13] considered three different configurations of methanol reactor at equilibrium condition: a once-through reactor, a reactor with the recycling of unconverted gases, and a reactor equipped with a membrane permeable to water. The feed flows were pure hydrogen and carbon dioxide. They showed that if a reactor with the recycle of unconverted gases is employed for methanol production, the highest carbon conversion of 69% is achievable. Atsonios et al. [14] evaluated the effect of different design and operating criteria on the carbon-to-methanol conversion system. They concluded that hydrogen production cost is the most significant parameter. Rivarolo et al. [15] studied the thermoeconomic performance of high-pressure reactors for methanol production when different renewable energy resources are employed. Their results depicted that biogas-based plant has the best economic performance, and purchasing carbon dioxide leads to lower capital investment. Nami et al. [16] investigated the performance of a power, methanol, and hydrogen production unit from thermodynamic, thermoeconomic, and environmental viewpoints. Their proposed design consisted of a geothermal driven organic Rankine cycle, a proton exchange membrane electrolyzer (PEME), an oxy-fuel combustion S-Graz cycle, and a methanol synthesis unit. They pointed out that the most crucial part of the system for investment was the S-Graz cycle, and the product unit cost was estimated at around 24.88 $/GJ. Kiatphuengporn et al. [17] studied the effect of an external magnetic field on the performance of a packed reactor in which methanol was produced through carbon dioxide hydrogenation. The reactor was filled with copper-iron-supported catalysts. Their results showed that applying a magnetic field enhanced reactor efficiency, carbon dioxide conversion, and methanol generation. Luu et al. [18] evaluated a post-combustion carbon capture system for enhanced gas recovery and methanol production from the flue gas of a coal-fired power plant. They claimed that their proposed design could operate well based on natural gas with high carbon dioxide concentration. Charoensuppanimit et al. [19] analyzed the possibility of using hydrogen from the Sodium methoxide ($NaOCH_3$) generation process in the carbon dioxide hydrogenation reaction. They reported that an adiabatic packed bed reactor was the best option. Ghosh et al. [20] evaluated three process schemes for methanol production from the generated carbon dioxide in a biogas plant. They demonstrated that all designs could provide their electricity demand and the two-reactor plan with fibrous catalyst has the highest efficiency and methanol yield. Gao et al. [21] proposed two options to set syngas ratio in the methanol generation process from landfill gas; providing additional hydrogen or separating extra carbon dioxide in landfill gas. They concluded that the first option is energy efficient, while the second one is more economical. Alsayegh et al. [22] investigated a new methanol production scheme in which captured carbon dioxide safely dilutes the produced hydrogen from photovoltaic water splitting and facilitates the hydrogenation reaction. Their economic evaluation revealed that generated methanol, in this case, is more expensive than the conventional ones. Matzen et al. [23] simulated a methanol and dimethyl ether production unit from wind-based electrolytic hydrogen and separated carbon dioxide from an ethanol ($C_2H_5OH$) fermentation system. They reported that although the environmental effect of methanol generation is less than dimethyl ether, its combustion offsets these benefits.

From the literature review in the previous paragraph, it can be concluded that many researchers have evaluated different schemes for methanol production from flue gas carbon dioxide. However, it seems more study and investigation are necessary in this field to identify proper applicable designs for various conditions. In this paper, a new methanol, hydrogen, and power trigeneration system is proposed and analyzed from the thermodynamic viewpoint. As it is well known, flue gas from refinery furnaces contains a considerable amount of carbon dioxide. So, a $CO_2$-to-methanol conversion system is considered to prevent carbon release into the surrounding atmosphere. The water-splitting reaction in the proton exchange membrane electrolyzer provides the necessary hydrogen for carbon hydrogenation. A solar energy collecting system is integrated to supply PEME power requirements. A part of the produced hydrogen is used in the methanol generation process, and the remainder is stored to be used in cloudy or night times or sold as a valuable byproduct. The main improvements of the proposed system can be highlighted as follow:

- An organic Rankine cycle is used to produce power from the flue gas energy content and adjust its temperature for the carbon capture unit.
- A part of the produced methanol is used in a direct methanol fuel cell to generate a stable and accessible electrical power for nearby buildings. Hence, it is not necessary to store and transport methanol to remote places for further processing.
- The electrochemical and thermodynamic performances of direct methanol fuel cell are simulated based on Aspen HYSYS available components and blocks. To the authors' knowledge, this has not been done so far.
- Special attention is paid to heat and stream integration among different components of the system. Hence, the external heat requirements will be as low as possible. Also, depleted stream decreases significantly.
- The produced flue gas in the methanol synthesis unit contains carbon dioxide. So, it is returned to the starting point of the system. Thus, no carbon dioxide is emitted to the environment.

By applying the first and second laws of thermodynamics and necessary supplementary equations for each subsystem, the energy and exergy operation of the proposed system is simulated in Aspen HYSYS environment and Engineering Equation Solver (EES) software, respectively. Then, the performance of each subsystem is studied under various operating conditions.

## 2. System description

The proposed methanol, hydrogen, and power trigeneration system consists of five subsystems: organic Rankine cycle (ORC), $CO_2$ capture unit (CC), proton exchange membrane electrolyzer (PEME), methanol synthesis unit (MSU), and direct methanol fuel cell (DMFC). An overview of the whole system is shown in Fig. 1. Aspen HYSYS v8.8 with three different fluid packages is used to design and simulate the system. Acid Gas and Extended NRTL fluid packages are used for the $CO_2$ capture and methanol synthesis units, respectively. While for the rest of the units, the Peng-Robinson fluid package is used. The detailed configuration of the system in the Aspen HYSYS simulation environment is depicted in Fig. 2. The streams entering the system are flue gas, water, and air. The flue gas considered for treating is the outlet of conventional refinery furnaces at the temperature of 220 °C and a total flow rate of 250,194 $m^3$/h with the mentioned composition in Table 1.

Exhaust flue gas from refinery furnaces stack is at high temperature and contains a lot of energy. So, it can be used to drive ORC for power generation, which can be used in other parts of the system. Also, the temperature of the flue gas decreases to such an extent that it is suitable for the carbon capture unit. After this step, the flue gas enters the carbon capture unit, where about 91% of $CO_2$ is captured, and the rest is emitted into the atmosphere. This captured carbon is sent to the methanol synthesis unit. However, a considerable amount of hydrogen is needed to implement the methanol synthesis reaction. In this case, hydrogen is

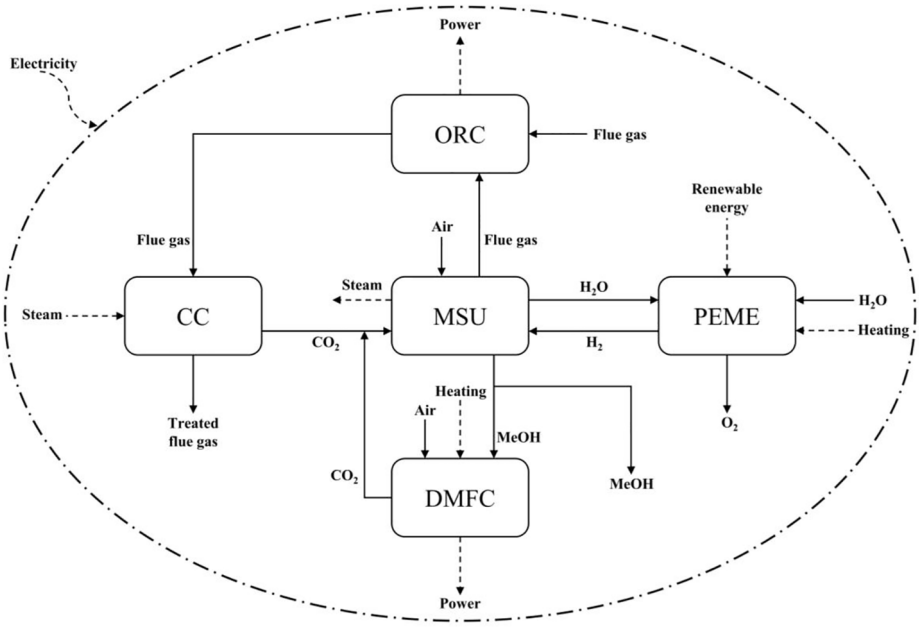


**Fig. 1.** An overview of the whole system.

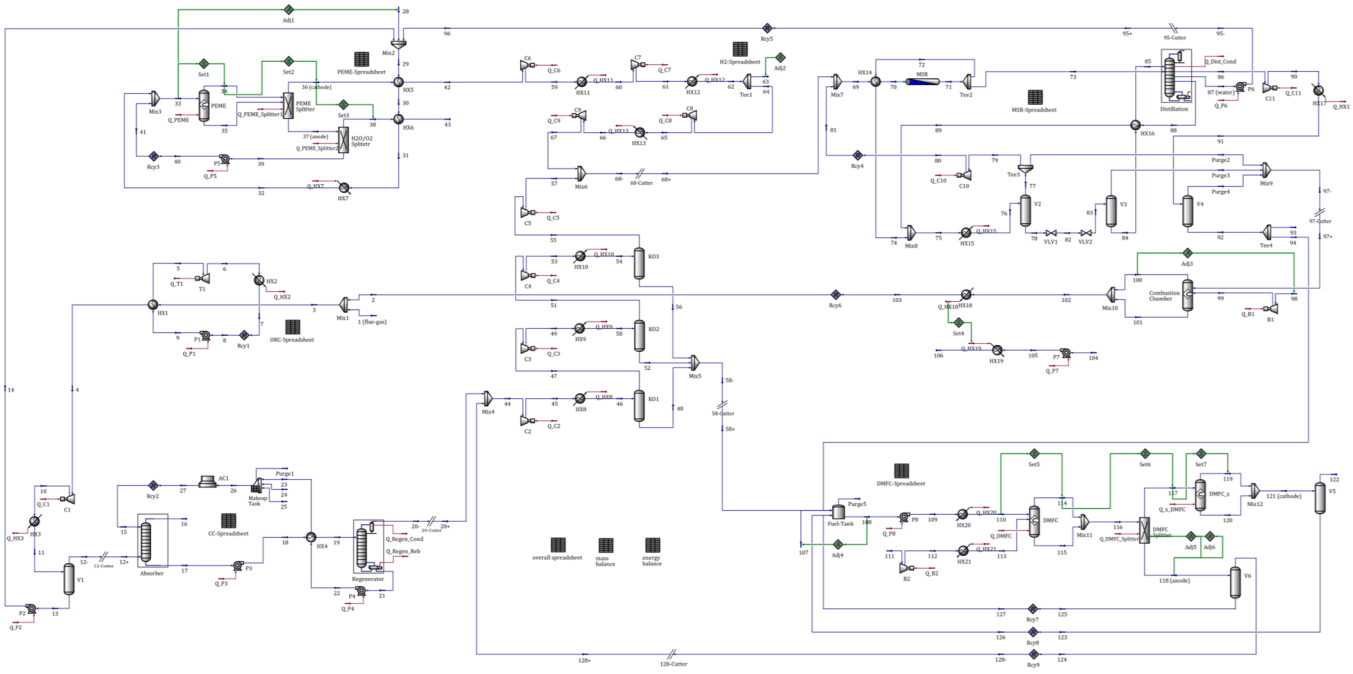

**Fig. 2.** Configuration of the system in Aspen HYSYS.

**Table 1**
Molar composition of inlet flue gas to the system.

| Composition | Molar fraction |
|---|---|
| $N_2$ | 0.782 |
| $O_2$ | 0.021 |
| $H_2O$ | 0.074 |
| $CO_2$ | 0.123 |

produced in the proton exchange membrane electrolyzer through the water-splitting reaction. A solar energy collector provides the PEME necessary power. Part of the produced hydrogen is sent to MSU, and the rest is stored as a byproduct. In the methanol synthesis unit, carbon dioxide and hydrogen react to produce methanol and water. Water is recycled back to the electrolyzer for hydrogen generation. A part of methanol is sent to a direct methanol fuel cell stack for power generation, while the remainder is stored as a liquid fuel for later usage or sale. Finally, combusting the vented gas from the methanol synthesis unit provides enough heat for high pressure steam generation, which is a useful energy source and can be used in the system if necessary. The performance of each subsystem is described in detail in the following sections.

The following assumptions are applied to simulate the designed system:

- The whole system operates at a steady-state condition.

- The pressure changes in the pipelines are neglected.
- There are no heat losses from pipelines and equipment.
- The cooling fluid used in the system is cooling water with temperature and pressure of 25 °C and 3 bar.
- The adiabatic efficiency of all rotating equipment (pump, compressor, and turbine) is considered 85%.
- There is no temperature change inside the electrolyzer and fuel cell.
- The changes in potential and kinetic energy and exergy are neglected.
- Ambient temperature and pressure are 25 °C and 1 atm, respectively.

### 2.1. Organic Rankine cycle subsystem

As stated previously, the exhaust flue gas from a refinery furnaces stack is too hot to enter the carbon capture unit directly. Hence, an organic Rankine cycle is considered to decrease flue gas temperature and utilize its large energy content. It is proven that organic Rankine cycles are more reliable, less complicated, and more suitable for waste heat recovery than Rankine cycles [24,25]. Various working fluids can be considered for ORC. Here, Refrig-600 is selected because it has a high critical temperature, better performance, and efficiency considering the thermal economic, safety, and environmental criteria. The physical properties of Refrig-600 are listed in Table 2 [26].

The schematic of the simulated organic Rankine cycle in Aspen HYSYS is presented in Fig. 3. As it is shown, this subsystem consists of a feed pump, an evaporator, an expander, and a condenser. Exhaust flue gas from the refinery furnace stack (stream 1) and flue gas from the purge streams boiler (stream 2) are mixed and sent to the shell side of the ORC evaporator (HX1). Refrig-600 exchanges heat with the flue gas and becomes superheated. Then, it enters the expander (T1) at 110 °C to generate power. The working fluid should become liquid to complete the cycle. This step is done by a cooler (HX2) in which Refrig-600 exchanges heat with cooling water. Thus, the temperature and pressure of the working fluid return to the pump suction conditions (stream 8), which are 30 °C and 3 bar, respectively.

The net generated power and thermal efficiency of ORC can be defined as:

$$W_{net,ORC} = W_{T1} - W_{P1} \tag{1}$$

$$\eta_{ORC} = \frac{W_{net,ORC}}{Q_{HX1}} \tag{2}$$

### 2.2. Carbon capture subsystem

The amine process is the most proven technique for recovering carbon dioxide from flue gases. In this process, $CO_2$ is chemically absorbed by the amine solution. The simulated carbon capture unit with Aspen HYSYS is presented in Fig. 4 based on the configuration of [27]. The rate of capturing $CO_2$ is 90.74%, and about 29.97 t/h of $CO_2$ is produced at a temperature of 35 °C and a pressure of 1.7 bar.

According to Fig. 4, outlet flue gas from the ORC evaporator's shell side enters compressor C1 to compensate for the pressure drop of the carbon capture unit absorber. The outlet stream of the compressor (stream 10) is cooled down to 45 °C with cooling water before entering the absorber. Hence, partial dehumidification occurs. A part of water vapor (about 445.50 kg/h) in the flue gas is condensed, separated at separator V1, and pumped through P2 to the electrolyzer unit for hydrogen generation. Now, the flue gas (stream 12) is ready to enter the carbon capture unit.

**Table 2**
Some physical properties of Refrig-600.

| Parameter | Value | Unit |
|---|---|---|
| Molecular weight | 58.12 | g/mol |
| Critical temperature | 151.98 | ℃ |
| Critical pressure | 3.80 | MPa |
| Latent heat of vaporization at b.p. | 366.35 | J/g |
| Flammable limits in air | 1.8–8.4 | % vol |

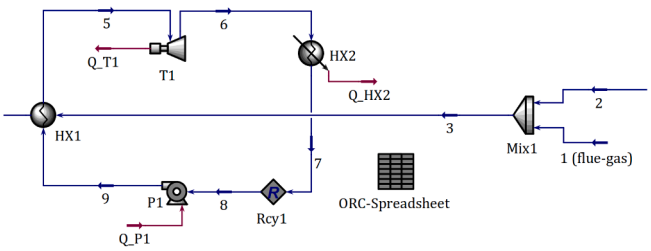


**Fig. 3.** Schematic of simulated ORC in Aspen HYSYS.

The $CO_2$-rich flue gas is fed to the bottom of the absorber column, while lean aqueous solvent with 30% wt MEA ($HOCH_2CH_2NH_2$) enters the column's top. The flue gas rises through the absorber column while the MEA descends, leading to direct counter-current contact between $CO_2$ and MEA. The reactions occurring in the absorber column are listed below [27]:

$$2H_2O \leftrightarrow H_3O^+ + OH^- \tag{3}$$

$$CO_2 + OH^- \rightarrow HCO_3^- \tag{4}$$

$$H_2O + HCO_3^- \leftrightarrow H_3O^+ + CO_3^{2-} \tag{5}$$

$$HCO_3^- \rightarrow CO_2 + OH^- \tag{6}$$

$$MEA + H_2O + CO_2 \rightarrow MEACOO^- + H_3O^+ \tag{7}$$

$$MEACOO^- + H_3O^+ \rightarrow MEA + H_2O + CO_2 \tag{8}$$

$$MEAH^+ + H_2O \rightarrow MEA + H_3O^+ \tag{9}$$

By implementing these reactions, $CO_2$ is chemically absorbed by MEA and is separated from flue gas. The treated flue gas with a low concentration of $CO_2$ is emitted from the top of the column into the atmosphere. The rich solvent (stream 17) leaves the column at the bottom, is pumped to the pressure of 2.5 bar, and flows into the internal lean/rich heat exchanger (HX4). The hot regenerated lean MEA coming from the bottom of the regeneration column is used to heat the pressurized rich solvent. Then, the hot rich solvent enters the regenerator and receives heat from the reboiler steam to desorb its $CO_2$. The product of the regeneration column at the bottom is lean MEA, which undergoes the following units: It gets cool in the lean/rich exchanger (HX4), mixes with water and MEA make-ups, cools to 45 °C in the air cooler (AC1), and finally, goes back into the absorber column. In this way, the MEA loss because of thermal degradation and evaporation is compensated [28]. On the other hand, the regeneration column's top product is a mixture of $CO_2$ and $H_2O$, which is cooled down to 35 °C in the condenser. Hence, a part of water vapor condenses and returns to the regeneration column with a reflux ratio of 1.23. In Table 3, the main design characteristics for absorber and regenerator columns are listed.

### 2.3. Water electrolyzer subsystem

The most common method to produce hydrogen from water is the electrolysis process. Although the fundamental principle of water splitting is the same, it can be performed in three different electrolyzers: alkaline water electrolyzer (AE), proton exchange membrane water electrolyzer (PEME), and solid oxide water electrolyzer (SOE). Solid oxide electrolyzer is still in the research and development stage and does not have commercial applications [29]. Despite the mature technology of alkaline electrolyzer, the advantages of PEME, such as compact design

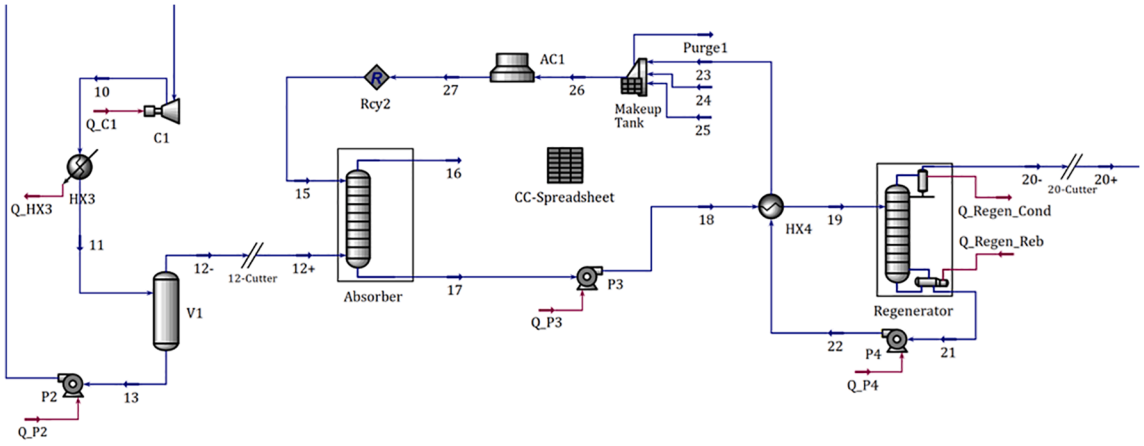


**Fig. 4.** Simulated carbon capture unit in Aspen HYSYS.

**Table 3**
Design characteristics of absorber and regenerator columns.

| Parameter | Absorber | Regenerator | Unit |
|---|---|---|---|
| Column diameter | 6 | 3 | m |
| Column height | 12.19 | 12.19 | m |
| Packing type | IMTP – metal (50 mm) | IMTP – metal (50 mm) | – |
| Reflux ratio | – | 1.23 | – |

[30], higher purity of produced gas [31], and higher current density and efficiency [32], make it an attractive and favorable choice for hydrogen production. In this study, a low-pressure polymer electrolyte membrane electrolyzer is considered for water splitting. The half-cell and overall reactions occurring inside the PEME are as follows:

$$anode: \quad H_2O \rightarrow 2H^+ + 2e^- + \frac{1}{2}O_2 \tag{10}$$

$$cathode: \quad 2H^+ + 2e^- \rightarrow H_2 \tag{11}$$

$$overall: \quad H_2O \rightarrow H_2 + \frac{1}{2}O_2 \tag{12}$$

Since there is no in-built module for PEME in Aspen HYSYS software, some process equipment is arranged to simulate the PEME. Fig. 5 shows the process flow diagram of the PEME subsystem in the Aspen HYSYS environment. It includes one conversion reactor for the electrolysis reaction, one component splitter for the separation of the anode and cathode flows, three SET logical operations (Set1, Set2, and Set3) for temperature matching of streams, and one component splitter for the separation of $H_2O$ and $O_2$ at the anode side.

According to Fig. 5, inlet water of PEME is the mixture of three streams: make-up fresh water (stream 28), separated water from flue gas by partial dehumidification (stream 14) and produced water in the methanol synthesis unit (stream 96). It is worth mentioning that the operating temperature of PEME is constant at 80 °C. So, for heat integration and increasing the system's efficiency, the inlet water stream is preheated with hydrogen and oxygen streams exiting the electrolyzer, and then it is heated in HX7 to reach the PEME temperature. Before entering the PEME, it is mixed with the unconverted water in the PEME outlet (stream 41). In the PEME reactor, the electrochemical water splitting reaction takes place. Then, hydrogen, oxygen, and the unconverted water are fed into the electrolyzer splitter so that the cathode stream is separated from the anode one. The cathode flow (stream 36) contains pure hydrogen at 80 °C, which cools down to 35 °C in HX5 and goes to the compression section of the methanol synthesis unit. The anode side flow (stream 37), a mixture of oxygen and water, is fed to another splitter to purify oxygen (stream 38) and recycle the unreacted water. The pure oxygen is cooled down in HX6 and is stored as a valuable byproduct to be sold if wanted. The unconverted water is returned to the electrolyzer after increasing its pressure through a pump.

Using Faraday's law, the molar flow rate of produced hydrogen and oxygen and consumed water are as follows:

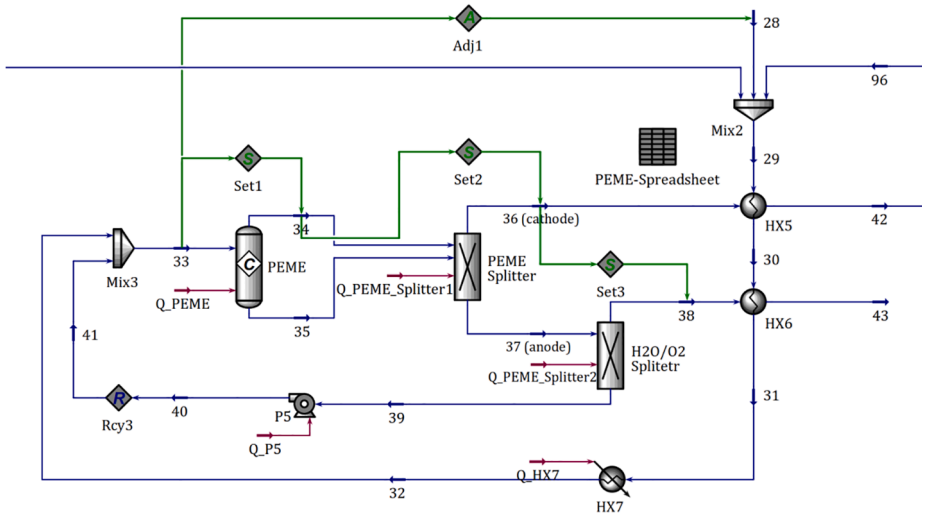


**Fig. 5.** Process flow diagram of simulated PEME subsystem in Aspen HYSYS.

$$\dot{N}^{cons}_{PEME,H_2O} = \frac{I}{2F} \tag{13}$$

$$\dot{N}^{prod}_{PEME,H_2} = \frac{I}{2F} \tag{14}$$

$$\dot{N}^{prod}_{PEME,O_2} = \frac{I}{4F} \tag{15}$$

The necessary amount of hydrogen for methanol synthesis can be calculated stoichiometrically (by using Adj2). In this regard, the PEME subsystem is designed to produce 25 t/h of hydrogen. About 17.5% of the generated hydrogen is used in the methanol synthesis unit. The rest is stored to provide energy in cloudy or night times or other urgent cases or can be sold as a valuable product.

Water electrolysis is a power-consuming process. So, it is necessary to determine PEME voltage and the rate of its required power. The following equation is used to calculate the necessary power of PEME:

$$W_{PEME,stack} = V_{stack}.I = V_{cell}.N.i.A_{cell} \tag{16}$$

The cell voltage for PEME can be expressed as:

$$V_{cell} = U_{rev} + v_{act,a} + v_{act,c} + v_{ohm} + v_{conc} \tag{17}$$

At low current densities, the concentration overpotential can be neglected [32]. The reversible or open-circuit potential can be determined using the Nernst equation [33]:

$$U_{rev} = U^0_{rev} + \frac{RT}{nF} ln\left(\frac{p_{H_2}\cdot\sqrt{p_{O_2}}}{a_{H_2O}}\right) \tag{18}$$

$$U^0_{rev} = 1.229 - 0.9 \times 10^{-3}(T - 298.15) \tag{19}$$

For water-splitting reaction, $n$ is 2, and $a_{H2O}$ is 1 for the liquid state.

The activation overpotential of anode and cathode can be calculated by simplifying the Butler-Volmer equation [34]:

$$v_{act,i} = \frac{RT}{\alpha_i F} sinh^{-1}\left(\frac{i}{2i_{0,i}}\right) \quad , \quad i = a, c \tag{20}$$

$$i_{0,i} = i^{ref}_i exp\left(\frac{-E_{act,i}}{RT}\right) \quad , \quad i = a, c \tag{21}$$

where the charge transfer coefficient for both anode and cathode is equal to 1 ($\alpha_a = \alpha_c = 1$).

The ohmic overpotential is mainly due to resistance to proton flow through the membrane and can be obtained from Ohm law [35]:

$$v_{ohm} = R_{mem}.i = \frac{\delta_{mem}}{\sigma_{mem}}.i \tag{22}$$

$$\sigma_{mem} = (0.5139\lambda - 0.326)exp\left[1268\left(\frac{1}{303.15} - \frac{1}{T}\right)\right] \tag{23}$$

$$\lambda = \frac{(-2.89556 + 0.016T) + 1.625}{0.1875} \tag{24}$$

The values of constant parameters used for PEME modeling are listed in Table 4.

**Table 4**
Parameters used for PEME modeling.

| parameter | Value | Unit | Refs. |
|---|---|---|---|
| $T$ | 80 | ℃ | – |
| $p_{H_2} = p_{O_2}$ | 1.5 | bar | – |
| $i^{ref}_a$ | 1744271.56 | A/m$^2$ | [34] |
| $i^{ref}_c$ | 4597.14 | A/m$^2$ | [34] |
| $E_{act,a}$ | 76 | kJ/mol | [34] |
| $E_{act,c}$ | 18 | kJ/mol | [34] |
| $\delta_{mem}$ | 50 | μm | [34] |

To evaluate the performance of the electrolyzer subsystem, its efficiency should be calculated, which is the ratio of produced hydrogen energy to total consumed power in the PEME stack:

$$\eta_{PEME} = \frac{\dot{M}_{H_2}.HHV_{H_2}}{W_{net}} \tag{25}$$

$$W_{net} = W_{PEME,stack} + Q_{HX7} + W_{P5} \tag{26}$$

where HHV is the higher heating value of hydrogen and equals 141.88 MJ/kg.

### 2.4. Methanol synthesis subsystem

In general, there are two methods for methanol production from carbon dioxide: 1) direct or one-step synthesis, in which $CO_2$ and $H_2$ are directly reacted, and methanol is generated, 2) indirect or two-step synthesis, where $CO_2$ first converts into CO through the reverse water gas shift (RWGS), and then methanol is produced. It has been shown that the direct method has higher economic and energy efficiency [36]. Therefore, the direct method for converting carbon dioxide to methanol is considered in this study. Synthesis of methanol is an exothermic reaction, and the following reactions co-occur in the reactor [7]:

$$CO_2 + 3H_2 \leftrightarrow CH_3OH + H_2O \quad , \quad \Delta H_{298.15} = -49.25\ (kJ/mol) \tag{27}$$

$$CO + 2H_2 \leftrightarrow CH_3OH \quad , \quad \Delta H_{298.15} = -90.7\ (kJ/mol) \tag{28}$$

$$CO_2 + H_2 \leftrightarrow CO + H_2O \quad , \quad \Delta H_{298.15} = +41.16\ (kJ/mol) \tag{29}$$

The first two reactions are the hydrogenation of $CO_2$ and CO to methanol (desired), respectively, and the third one is the reverse water gas shift (undesired). Following Le Chatelier's principle, the methanol synthesis reaction is favored by increasing pressure and decreasing temperature.

The proposed methanol synthesis unit in this paper is based on Van-Dal and Bouallou [37]. According to their work, the methanol synthesis has three main stages, including compression, reaction, and separation. The simulated methanol synthesis subsystem by Aspen HYSYS is depicted in Fig. 6.

This process is designed to produce 518.88 t/day methanol. At first, $CO_2$ and $H_2$ are compressed to 78 bar. It should be noted that $CO_2$ flow (stream 44) is the mixture of captured $CO_2$ from flue gas and produced $CO_2$ in the DMFC subsystem. It is fed at 1.013 bar and 34.8 °C. A series of four compressors with intercooling to 35 °C by cooling water is used to increase carbon dioxide pressure. These compressors (C2, C3, C4, and C5) are considered as reciprocating ones with a pressure ratio of about 3.16 and an adiabatic efficiency of 85%. Because the $CO_2$ stream is not pure and contains water vapor, part of this water is condensed after each intercooling and separated using knock-out drums (KO1, KO2, and KO3). These condensed streams are mixed and used in the DMFC subsystem. Similarly, $H_2$ (stream 42) is compressed from 1 bar and 35 °C to 78 bar through four reciprocating compressors (C6, C7, C8, and C9) with intercooling to 35 °C. The pressure ratio of these compressors is about 3.17, and their adiabatic efficiency is 85%. The outlet of the second compressor is divided into two streams after being cooled in HX12. One of these streams (stream 64) is used for methanol synthesis, while the other (stream 63) is sent to storage tanks.

The outlets of these compressors are mixed and, after mixing with recycled stream (stream 81), are preheated to 210 °C with a fraction of the reactor outlet (stream 72) in HX14, entering the reactor. Using the kinetics of reactions (27) to (29) as proposed in [37], the gases react over 15,975 kg of commercial $Cu/ZnO/Al_2O_3$ catalysts in an adiabatic fixed-bed plug flow reactor (MSR). For calculating the pressure drop inside the reactor, the Ergun equation was used. The reactor outlet (stream 71) contains hydrogen, carbon dioxide, methanol, water, and carbon monoxide and reaches the temperature of 287.9 °C because the reaction is exothermic. This stream is divided into two flows: Stream 72 is used to

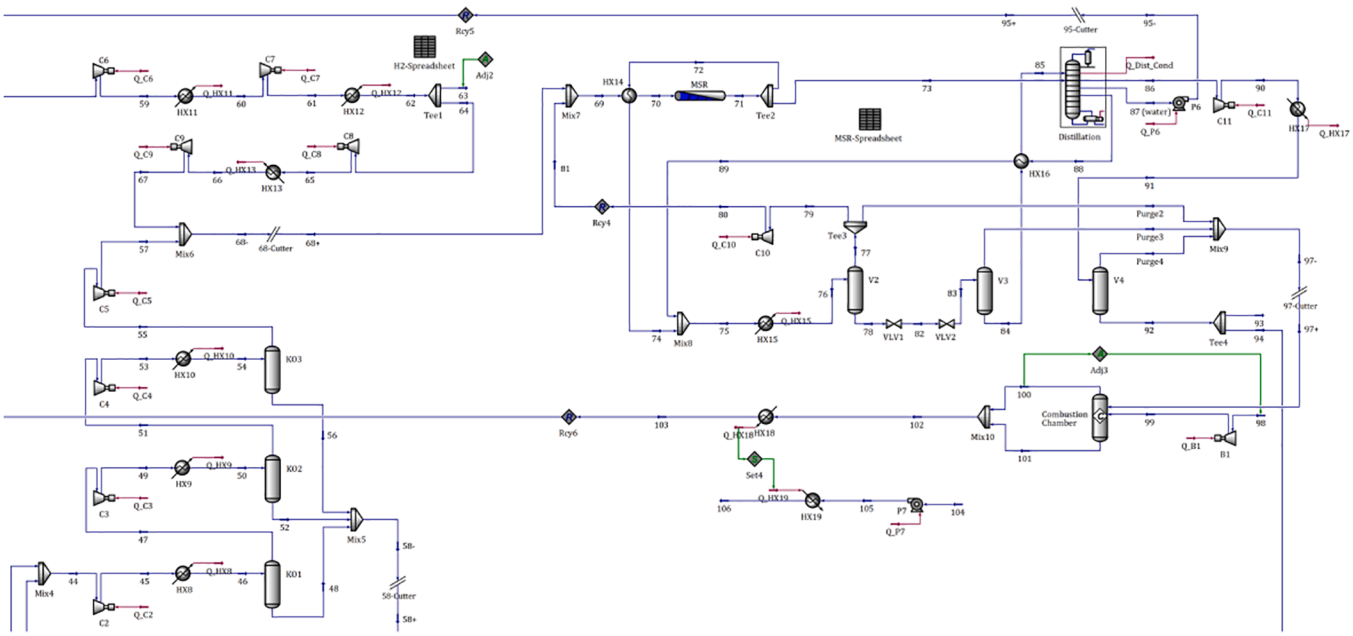


**Fig. 6.** Simulated methanol synthesis subsystem in Aspen HYSYS.

preheat the reactor feed in HX14, and stream 73 is used as a hot flow in the reboiler of the distillation column and in HX16. Through this heat integration, the temperature of these two streams decreases to around 83 °C, and then, they are remixed.

Besides, stream 75 cools down to 35 °C in HX15 using the cooling water. Thus, methanol and water are liquefied. This two-phase stream enters the flash drum (V2), where liquid methanol and water are separated from the unreacted gas. To prevent the accumulation of inert gases and byproducts in the reaction loop, 1% of unreacted gases are purged, and the remaining 99% are re-pressurized by the centrifugal compressor (C10) and recycled back to mix with a fresh feed of reactor inlet. The outflow stream from the bottom of the flash drum is throttled through two valves to 1.6 bar and then enters another flash drum (V3). The gas phase of drum V3 is purged, and its liquid phase, a mixture of methanol and water, is heated to 80 °C in HX16 and fed to the distillation column. The distillation column consists of 40 trays (fed at tray 25 from top), a partial condenser, and a reboiler. The reflux ratio of the column is 1.42, which leads to 50 $ppb_{wt}$ methanol in the bottom stream and 75 $ppm_{wt}$ water in the top product. The methanol in the top product stream is 99.86 wt% pure at vapor state. It is 64.1 °C but needs to be cooled to 35 °C and become liquid. Therefore, it is compressed to 1.2 bar with a centrifugal compressor (C11) and cooled using cooling water in HX17 and then enters the flash drum (V4) where remaining inert and unreacted gases are separated. The bottom product of the distillation column is pure water, so it is pumped through P6 to reach the pressure of the water electrolyzer subsystem.

It is better to reuse the purge streams, which contain valuable $H_2$, methanol, and CO to increase the efficiency of the methanol synthesis subsystem. Hence, the purge streams from V2, V3, and V4 are mixed and combusted with air in the boiler for steam generation. This steam can be used in the upstream carbon capture unit or elsewhere when needed. The boiler is modeled as one conversion reactor in which the combustion takes place. Two heat exchangers are considered for heat transfer between combustion gases and boiler feed water (BFW). Through Adj3, the inlet air flow rate to the boiler is adjusted to set the flame's temperature at 1250 °C. The combustion chamber outlet enters HX18 and generates 8547 kg/h high pressure steam at 380 °C and 42 bar. The efficiency of the boiler is set at 85% using Set4. The flue gas of the boiler (stream 2) is mixed with the system feed (stream 1), so its $CO_2$ content can be recovered in carbon capture unit. The combustion reactions in the boiler are as follow:

$$H_2 + \frac{1}{2}O_2 \rightarrow H_2O \tag{30}$$

$$CO + \frac{1}{2}O_2 \rightarrow CO_2 \tag{31}$$

$$CH_3OH + \frac{3}{2}O_2 \rightarrow CO_2 + 2H_2O \tag{32}$$

*Kinetics of reactions*. In this study, the modified kinetic model expressed in [37] is used for methanol synthesis, and RWGS rate calculations. Pressures are in Pa and temperatures are in K. These equations are as follows.

$$r_{CH_3OH} = \frac{k_1 p_{CO_2} p_{H_2} - k_6 \frac{p_{H_2O} p_{CH_3OH}}{p_{H_2}^2}}{\left(1 + k_2 \frac{p_{H_2O}}{p_{H_2}} + k_3 \sqrt{p_{H_2}} + k_4 p_{H_2O}\right)^3} \quad \left[\frac{kmol}{kg_{cat} s}\right] \tag{33}$$

$$r_{RWGS} = \frac{k_5 p_{CO_2} - k_7 \frac{p_{H_2O} p_{CO}}{p_{H_2}}}{1 + k_2 \frac{p_{H_2O}}{p_{H_2}} + k_3 \sqrt{p_{H_2}} + k_4 p_{H_2O}} \quad \left[\frac{kmol}{kg_{cat} s}\right] \tag{34}$$

$$lnk_i = A_i + \frac{B_i}{T} \quad , \quad i = 1:7 \tag{35}$$

The constants of these equations and characteristics of catalyst particles are shown in Table 5 and Table 6, respectively [37].

The thermodynamic performance of the methanol synthesis subsystem can be evaluated by various parameters. One of these parameters is carbon dioxide conversion and can be calculated in two ways: the $CO_2$

**Table 5**
Constants of the kinetic model.

| Index (i) | A | B |
|---|---|---|
| 1 | −29.87 | 4811.2 |
| 2 | 8.147 | 0 |
| 3 | −6.452 | 2068.4 |
| 4 | −34.95 | 14928.9 |
| 5 | 4.804 | −11797.5 |
| 6 | 17.55 | −2249.8 |
| 7 | 0.131 | −7023.5 |

**Table 6**
Characteristics of catalyst particles.

| Parameter | Value | Unit |
|---|---|---|
| Density | 1775 | kg/m$^3$ |
| Diameter | 5.5 | mm |
| Fixed bed porosity | 0.5 | – |

conversion in the reactor and the whole MSU.

$$X_{CO_2,i}(\%) = \left(\frac{\dot{N}^{in}_{CO_2} - \dot{N}^{out}_{CO_2}}{\dot{N}^{in}_{CO_2}}\right)_i \times 100 \quad , \quad i = reactor, unit \tag{36}$$

Methanol selectivity and methanol yield are the other thermodynamic metrics for MSU. Methanol selectivity is that fraction of consumed carbon dioxide that converts to methanol instead of other byproducts. Methanol yield is defined as the ratio of produced methanol in MSR to its inlet $CO_2$ as a raw material.

$$Selectivity_{CO_2}(\%) = \left(\frac{\dot{N}^{out}_{MeOH} - \dot{N}^{in}_{MeOH}}{\dot{N}^{in}_{CO_2} - \dot{N}^{out}_{CO_2}}\right) \times 100 \tag{37}$$

$$Yield_{CO_2}(\%) = \left(\frac{\dot{N}^{out}_{MeOH} - \dot{N}^{in}_{MeOH}}{\dot{N}^{in}_{CO_2}}\right) \times 100 \tag{38}$$

### 2.5. Direct methanol fuel cell subsystem

A part of the generated methanol can be used to generate stable power. The easiest way is to use a direct methanol fuel cell (DMFC), where liquid methanol solution is directly fed to the stack as the fuel. The most serious issue in this regard, which is unavoidable, is the crossover of the methanol from the membrane. Even with the most frequent type of electrolyte used in this type of fuel cell, methanol can dissolve it. This phenomenon lowers the performance and efficiency of the DMFC [38,39]. The electrochemical reactions at anode and cathode electrodes of DMFC and the overall reaction are as follows:

$$anode: \quad CH_3OH + H_2O \rightarrow 6H^+ + 6e^- + CO_2 \tag{39}$$

$$cathode: \quad \frac{3}{2}O_2 + 6H^+ + 6e^- \rightarrow 3H_2O \tag{40}$$

$$overall: \quad CH_3OH + \frac{3}{2}O_2 \rightarrow 2H_2O + CO_2 \tag{41}$$

The consumption and production rate of species in DMFC can be defined using Faraday's law:

$$\dot{N}^{cons}_{DMFC,MeOH,a} = \dot{N}^{cons}_{DMFC,H_2O,a} = \dot{N}^{prod}_{DMFC,CO_2,a} = \frac{I}{6F} \tag{42}$$

$$\dot{N}^{cons}_{DMFC,O_2,c} = \frac{I + I_{xover}}{4F} \tag{43}$$

$$\dot{N}^{prod}_{DMFC,H_2O,c} = \frac{3I + 2I_{xover}}{6F} \tag{44}$$

$$\dot{N}^{cons}_{DMFC,MeOH,c} = \frac{I_{xover}}{6F} \tag{45}$$

It is worthwhile to mention that the crossover methanol from the anode to the cathode through the membrane is completely consumed at the cathode side. This methanol crossover through the membrane is because of electro-osmotic drag (EOD) and diffusion. So, it can be concluded that:

$$\dot{N}^{cons}_{DMFC,MeOH,c} = \dot{N}^{cross}_{MeoH,mem} \tag{46}$$

$$\dot{N}^{cross}_{MeOH,mem} = \dot{N}^{eod}_{MeOH,mem} + \dot{N}^{diff}_{MeOH,mem} = n_{d,MeOH}\frac{I}{F} + D^{eff}_{MeOH,mem}\frac{C_{MeOH}|_{acl}}{\delta_{mem}}.N.A_{cell} \tag{47}$$

The EOD coefficient of methanol is a function of water EOD coefficient and methanol and water concentration in the anode catalyst layer [40]:

$$n_{d,MeOH} = n_{d,H_2O}\frac{C_{MeOH}}{C_{H_2O}}\bigg|_{acl} \tag{48}$$

$$n_{d,H_2O} = 1.6767 + 0.0155 \times (T - 273.15) + 8.9074 \times 10^{-5} \times (T - 273.15)^2 \tag{49}$$

Also, Bruggeman correlation is used for calculating the effective diffusion coefficient [40]:

$$D^{eff}_{MeOH,mem} = \varepsilon^{1.5} D_{MeOH,mem} \tag{50}$$

$$D_{MeOH,mem} = 4.9 \times 10^{-10} exp\left[2436\left(\frac{1}{333.15} - \frac{1}{T}\right)\right] \tag{51}$$

The generated electrical power by DMFC stack can be expressed as:

$$W_{DMFC,stack} = V_{stack}.I = V_{cell}.N.i.A_{cell} \tag{52}$$

where $V_{cell}$ is the cell voltage and can be obtained if all overpotentials are subtracted from the thermodynamic equilibrium voltage:

$$V_{cell} = U_{rev} - v_{kin,a} - v_{kin,c} - v_{ohm} - v_{cont} \tag{53}$$

The kinetic of the methanol oxidation reaction (MOR) expressed by Meyers and Newman [41] is used for calculating the electrochemical reaction rate at the anode side. On the other hand, the first-order Tafel-based kinetic [42] is used for oxygen reduction reaction (ORR) at the cathode side. For both anode and cathode, the charge transfer coefficient is equal to 0.5 ($\alpha_a = \alpha_c = 0.5$):

$$anode\ MOR: \quad i = i_{0,a}\frac{C_{MeOH}|_{acl} exp\left(\frac{\alpha_a F}{RT} v_{kin,a}\right)}{C_{MeOH}|_{acl} + K_{reac} exp\left(\frac{\alpha_a F}{RT} v_{kin,a}\right)} \tag{54}$$

$$cathode\ ORR: \quad i + i_{xover} = i_{0,c}\left(\frac{C_{O_2}|_{ccl}}{C^{ref}_{O_2}}\right) exp\left(\frac{\alpha_c F}{RT} v_{kin,c}\right) \tag{55}$$

The exchange current densities for the anode and the cathode sides are given by [43]:

$$i_{0,i} = i^{ref}_i exp\left[\frac{E_{act,i}}{R}\left(\frac{1}{353.15} - \frac{1}{T}\right)\right] \quad , \quad i = a, c \tag{56}$$

By rearranging equations (54) and (55), the values of kinetic losses due to the MOR and ORR can be obtained:

$$v_{kin,a} = \frac{RT}{\alpha_a F} ln\left(\frac{iC_{MeOH}|_{acl}}{i_{0,a}C_{MeOH}|_{acl} - iK_{reac}}\right) \tag{57}$$

$$v_{kin,c} = \frac{RT}{\alpha_c F} ln\left[\frac{i + i_{xover}}{i_{0,c}}\left(\frac{C^{ref}_{O_2}}{C_{O_2}|_{ccl}}\right)\right] \tag{58}$$

The membrane ohmic overpotential can be calculated by equation (22), as described in the electrolyzer subsystem, where:

$$\sigma_{mem} = (0.5139\lambda - 0.326) exp\left[1268\left(\frac{1}{333.15} - \frac{1}{T}\right)\right] \tag{59}$$

Finally, the contact resistance overpotential can be obtained from the following equation:

$$v_{cont} = iR_{cont} \tag{60}$$

The cell efficiency of DMFC is the product of three types of efficiency

- the theoretical one ($\eta_{th}$), the voltage one ($\eta_{volt}$) and the fuel one ($\eta_{fuel}$):

$$\eta_{cell} = \eta_{th}\eta_{volt}\eta_{fuel} \tag{61}$$

$$\eta_{th} = \frac{\Delta G}{\Delta H} \tag{62}$$

$$\eta_{volt} = \frac{V_{cell}}{U_{rev}} \tag{63}$$

$$\eta_{fuel} = \frac{i}{i + i_{xover}} \tag{64}$$

While for calculating the overall efficiency of the stack, the following equation should be used:

$$\eta_{DMFC} = \frac{W_{DMFC,stack}}{W_{net}} \tag{65}$$

$$W_{net} = \dot{M}_{MeOH}.HHV_{MeOH} + Q_{HX20} + Q_{HX21} + W_{P8} + W_{B2} \tag{66}$$

The value of HHV for methanol equals 22.7 MJ/kg. Table 7 lists the values of constant parameters used for modeling of DMFC in Aspen HYSYS.

Like PEME, the fuel cell is not a standard pre-defined component in Aspen HYSYS. So DMFC is developed using a series of in-built process equipment that can provide a similar process. The DMFC relevant flowsheet is depicted in Fig. 7. This developed model consists of two conversion reactors: the first one for the overall reaction and the second one for the reaction occurring at the cathode side because of methanol crossover. Moreover, one component splitter for separating the anode and cathode sides, three SET logical operations (Set5, Set6, and Set7) for matching streams temperature, and two adjust logical operations (Adj5 and Adj6) for adjusting the split fraction between anode and cathode streams are integrated into DMFC stack.

As shown, 3277.71 kg/h of methanol stream, which is about 15% of the total produced methanol in MSU, is sent to the DMFC subsystem. The considered inlet concentration of methanol in the DMFC stack is 2 M. So pure methanol is diluted in a fuel-tank where five streams are mixed: Stream 94 (main methanol from MSU), stream 58 (liquid outlet from $CO_2$ compression Knock-out drums), streams 126 and 127, which are liquid outlets from flash drums of DMFC cathode and anode sides, respectively, and stream 107 (pure water). The flow rate of pure water inlet is adjusted through Adj4 so that the concentration of the outlet stream from the fuel-tank becomes the desired one.

The prepared fuel enters the pump (P8) to compensate for the pressure drop in the subsequent heat exchanger. Parallel to the methanol solution, the needed air at the cathode side is sucked from the atmosphere employing the blower. These two streams enter the fuel cell stack after being heated to 50 °C (operating temperature of DMFC) in HX20 and HX21. Here, the overall reaction of DMFC takes place. Outlet streams of the reactor enter the DMFC splitter, where the components are split into anode and cathode streams. Adj4 and Adj5 set the split fractions inside the splitter so that the consumption and production rates of species are balanced. The anode stream (stream 118), which contains produced $CO_2$ alongside unreacted methanol and water, is fed to the flash drum (V6), and its liquid and gas phases are separated. The liquid phase is recycled back to the fuel tank, while the gas phase, which is mainly carbon dioxide (stream 128), is sent back to the suction of $CO_2$ compressors in the MSU. The cathode stream (stream 117) consists of air, produced water, and crossed over methanol. This methanol reacts completely on the cathode side, according to equation (41). The outlet stream of the cathode side (stream 121) is fed to the flash drum (V5), in which its gaseous phase is vented to the atmosphere, while its liquid phase (stream 126) is recycled back to the fuel tank.

**Table 7**
Parameters used for DMFC simulation.

| parameter | value | Unit | Ref. |
|---|---|---|---|
| T | 50 | ℃ | – |
| p | 1 | atm | – |
| $\varepsilon$ | 0.5 | – | [38] |
| $i_a^{ref}$ | 94.25 | A/m$^2$ | [43] |
| $i_c^{ref}$ | 0.0422 | A/m$^2$ | [43] |
| $E_{act,a}$ | 35,570 | J/mol | [43] |
| $E_{act,c}$ | 73,200 | J/mol | [43] |
| $K_{reac}$ | 0.2 | 1/s | [44] |
| $C_{O_2}^{ref}$ | 0.472 | mol/m$^3$ | [40] |
| $\delta_{mem}$ | 50 | μm | [38] |
| $R_{cont}$ | 0.45 × 10$^{-4}$ | Ωm$^2$ | [45] |

## 3. System analysis

After arranging the subsystems with optimum heat and mass interaction in the overall multigeneration system, all equations in the previous section with mass and energy conservation laws are implemented. Also, exergy analysis, originating from the second law of thermodynamics, is applied for each subsystem. Finally, defining energy and exergy efficiencies ensures a comprehensive investigation of the proposed system.

The second law of thermodynamic introduces the exergy concept. Exergy is the maximum obtainable work of a system as it passes from its initial state to a dead state and doing heat and work interactions only with its surroundings. In other words, exergy is the minimum work required to change the system from a dead state to a chosen state. So, the exergy analysis of a system or process detects the quantity and origin of energy losses, which is unattainable with energy analysis. Since energy resources are limited, and their optimal use is necessary, exergy analysis has gained great attention. It can be used to design new systems and optimize existing plants, so energy waste is decreased as much as possible.

If electrical, magnetic, nuclear, and surface tension effects, besides kinetic and potential exergy changes, are neglected, the exergy of a stream is the sum of its physical and chemical exergies:

$$\dot{E} = \dot{E}_{ph} + \dot{E}_{ch} \tag{67}$$

The physical exergy of a stream is the maximum possible work obtained when it changes reversibly from its initial state to the limited dead or environmental state:

$$\dot{E}_{ph} = \sum \dot{N}_i \left[ \left( \overline{h}_i - \overline{h}_i^{amb} \right) - T_{amb} \left( \overline{s}_i - \overline{s}_i^{amb} \right) \right] \tag{68}$$

The chemical exergy of a stream is the maximum work attained when it changes from a limited dead state to the real dead state. For an ideal gas mixture, the chemical exergy is calculated as:

$$\dot{E}_{ch} = \sum \dot{N}_i \overline{e}_i^{ch} + RT_{amb} \sum \dot{N}_i ln y_i \tag{69}$$

The exergy balance of a component under steady-state condition can be written as:

$$\dot{E}_{des,k} = \sum_j \left( 1 - \frac{T_{amb}}{T_j} \right) Q_j - W_{cv} + \sum_{in} \dot{E}_{in} - \sum_{out} \dot{E}_{out} \tag{70}$$

The equation mentioned above states that the system inlet exergy is more than its outlet exergy since the irreversibilities cause some exergy destruction.

As shown in Fig. 1, all the subsystems interact to produce the desired products with maximum heat and material recovery. The overall system can be considered as one control volume operating at a steady state. In this case, the overall system's energy efficiency can be defined as the ratio of the whole valuable products to the total amount of useful inputs. The outputs of the system are: the power of ORC turbine; produced power of DMFC; stored hydrogen in stream 63; generated methanol in

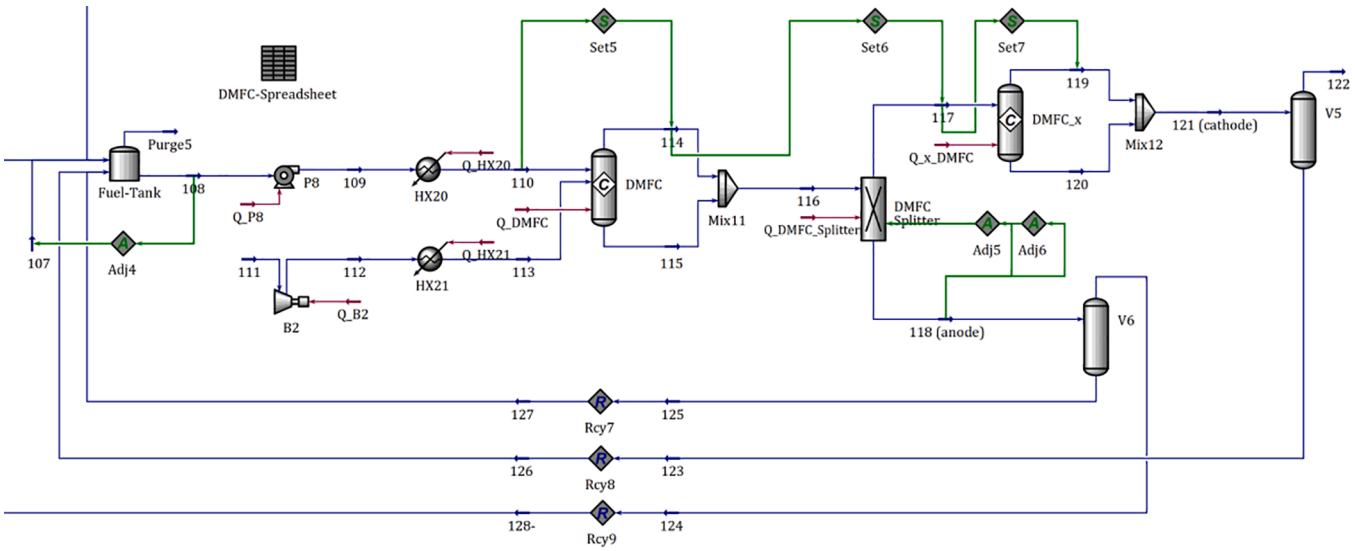


**Fig. 7.** Process flow diagram of simulated DMFC subsystem in Aspen HYSYS.

**Table 8**
Comparison of the proposed trigeneration system plant to other systems.

| Case study | System type | Fuel | Application | Advantageous | Drawbacks | Efficiencies |
|---|---|---|---|---|---|---|
| Present work | Trigeneration methanol, hydrogen, and power system | Flue gas and solar energy | - Commercial application- Small industries | - Reduction in emitted $CO_2$- Additional power generation- methanol and hydrogen production by carbon capture | - Solar panels may be expensive- The system is bulky | - Energy efficiency = 66.84%- Exergy efficiency = 55.10% |
| Boretti [10] | Methanol production system | Carbon dioxide from oxy-fuel combustion and solar/wind renewable energy | Industrial use | - Reduction in environmental carbon pollutant- Methanol seems a better, safer, and easier option than hydrogen for transportation, distribution, and small/ high power density utilization | A significant amount of renewable energy is necessary | – |
| Sayah et al. [11] | Methanol production system | Flue gas and wind energy | Commercial application | - Zero carbon emission- Methanol production- Compatibility with Iran condition- Can compete with conventional methanol synthesis options- Lowering methanol and steam intensity- Lower cost | - The detailed cost estimation depends on the energy source- A separate unit for methanol synthesis affects the product cost | – |
| Esmaili et al. [12] | Hydrogen and methanol production system | Carbon dioxide and solar energy | Commercial and industrial applications | - Zero carbon emission- Compact structure- Improved efficiency | - Heat and water management should be considered- Dependent on solar radiation | Energy and exergy efficiencies = 55%-90% |
| Atsonios et al. [14] | Methanol production system | Flue gas and electricity from the grid or renewable energy source | Commercial application | - Lowering carbon dioxide emission- Additional power generation with a Power-to-fuel integrated system | - Hydrogen production cost has a significant impact- Carbon dioxide-based fuels do not share much in the global market | – |
| Rivarolo et al. [15] | Methanol production system | Solar/wind/ hydroelectric energy and biogas/external plant carbon dioxide | Industrial application | - Zero carbon emission- No fossil fuel consumption for hydrogen generation- Biogas configuration has the best performance | - The presented configurations do not seem viable yet- If any interruption happens in providing renewable energy, the necessary power should be extracted from the grid- The renewable sources are not available throughout the year | – |
| Nami et al. [16] | Methanol, hydrogen, and power production system | Carbon dioxide from the S-Graz cycle and renewable hydrogen | Industrial application | - Zero-emission- Good equipment integration | The cost is the main factor | – |
| Alsayegh et al. [22] | Methanol production system | Carbon dioxide and solar energy | Industrial application | - Simplicity- Zero carbon emission | - Special attention should be paid to heat and hydrogen to carbon ratio management- Further research and investigations are needed | Energy efficiency = 28.18% |
| Matzen et al. [23] | Methanol and dimethyl ether cogeneration system | Carbon dioxide from the ethanol fermentation process and wind-based hydrogen | Commercial application | - Lower carbon dioxide emission- Renewable energy usage | - Its feasibility is under doubt- System complexity | – |

stream 93; and produced steam. Also, the overall system's inputs are the consumed power of all compressors and pumps; the necessary power of water electrolyzer; and consumed steam for heating. Hence, the energy efficiency of the proposed multigeneration system can be defined as:

$$\eta_{overall} = \frac{W_{T1} + W_{DMFC,stack} + \dot{M}_{H_2}.HHV_{H_2} + \dot{M}_{MeOH}.HHV_{MeOH} + Q^{prod}_{steam}}{W^{tot}_{C} + W^{tot}_{P} + W_{PEME,stack} + Q^{cons}_{steam}} \quad (71)$$

Likewise, exergy efficiency is defined as:

$$\eta_{exergy} = \frac{W_{T1} + W_{DMFC,stack} + \dot{N}_{H_2}.\overline{e}^{ch}_{H_2} + \dot{N}_{MeOH}.\overline{e}^{ch}_{MeOH} + Q^{prod}_{steam}\left(1 - \frac{T_{amb}}{T^{prod}_{b,steam}}\right)}{W^{tot}_{C} + W^{tot}_{P} + W_{PEME,stack} + Q^{cons}_{steam}\left(1 - \frac{T_{amb}}{T^{cons}_{b,steam}}\right)} \quad (72)$$

## 4. Results and discussion

In this section, the results of the base case and parametric studies are presented and discussed in detail. The proposed trigeneration system in this paper is compared to other systems with various fuels or prime movers in Table 8 that shows relatively better performance.

### 4.1. Base case

Table 9 and Table 10 show the mass and energy balance for the proposed system, respectively. According to Table 9, a tremendous amount of oxygen is produced in the PEM electrolyzer through water splitting. As listed in Table 10, the PEM electrolyzer has the highest share in the system power consumption rate. On the other hand, ORC power consumption is the lowest. Also, the conditions of the streams are listed in Table 11.

In Table 12, the main performance parameters of the subsystems and overall system are given. The overall system's energy and exergy efficiencies in the base case condition are 66.84% and 55.10%, respectively.

Fig. 8 reveals the share of each subsystem in the total exergy destruction rate. As can be seen, the PEME subsystem has the highest effect on the system exergy destruction, which is mainly due to its enormous power consumption rate. However, ORC owns a negligible share because there is no reaction in it.

### 4.2. Parametric study

#### 4.2.1. Organic Rankine cycle

Fig. 9 shows the effect of changing turbine inlet pressure on ORC efficiency for different values of turbine inlet temperature. It is worth mentioning that the outlet temperature of flue gas from the evaporator is constant. According to this figure, at a constant turbine inlet temperature, an increase in the turbine inlet pressure leads to a rise in ORC efficiency. As the flue gas temperature is unchanged, the input energy of ORC, $Q_{HX1}$, is constant. Higher turbine inlet pressure means more turbine power production and pump power consumption. The overall result is the increase of the ORC net generated power and, consequently, ORC efficiency. Furthermore, ORC efficiency decreases as the turbine inlet temperature increases for a definite turbine inlet pressure. The ORC cycle flowrate decreases when the turbine inlet temperature increases since ORC input energy is constant. Hence, the turbine generated power, ORC net power, and cycle efficiency decrease by selecting a higher turbine inlet power.

**Table 9**
Mass balance.

| Component | In (t/h) | Out (t/h) |
|---|---|---|
| $CO_2$ | 31.38 | 5.66 |
| $H_2$ | 0 | 20.61 |
| MeOH | 0 | 18.34 |
| $H_2O$ | 249.5 | 44.4 |
| CO | 0 | 0.0004 |
| $O_2$ | 28.41 | 219.86 |

#### 4.2.2. Carbon capture

The temperature and gas-phase $CO_2$ molar flowrate profiles inside the absorber column are shown in Fig. 10. As expected, the $CO_2$ flowrate decreases while moving up the absorber column due to the carbon capture process. The absorption rate is fast at the bottom stages, but it gets slow at the upper stages since carbon removal approaches its maximum value and equilibrium condition. Meanwhile, temperature increases at first and reaches its maximum value (73.97 °C) at stage 4, and decreases afterward. The shape of the temperature profile and its peak depends on such parameters as the liquid to gas ratio, solvent properties, the heat of absorption reaction, column height, and carbon concentration in the flue gas [46].

#### 4.2.3. Water electrolyzer

To ensure that the simulation of PEME in Aspen HYSYS software is done correctly, the V-i curve of PEME in this work is compared with data reported in [47] and is depicted in Fig. 11. This figure indicates a good agreement between them, and the maximum relative error is 1.4%. So, it can be concluded that the PEME simulation block in this work can predict electrolyzer performance precisely.

Heat demand of PEME, i.e., TΔS, and its heat generation due to irreversibilities, i.e., overpotentials, are demonstrated in Fig. 12. According to this figure, generated heat increases with current density because activation and ohmic overpotential terms directly relate to the electrolyzer current density (Eqs. (20), 22). Moreover, it is observed that in all values of current density, PEME heat demand is less than its produced heat. Hence, there is no need to provide extra heat from any external source, and the excess heat should be emitted to keep the PEME at a constant temperature.

Fig. 13 shows the effect of current density on the electrolyzer electrical power input and the generated hydrogen energy output. It is evident that both energy input and energy output increase with increasing electrolyzer current density. However, the rate of power demand increase is much higher than that of produced hydrogen. It leads to PEME energy efficiency reduction, as depicted in Fig. 14. Energy efficiency decreases more rapidly when i less than 1000 A/m$^2$. Afterward, it has a linear reduction approach. Also, referring to Fig. 14, electrolyzer voltage gets higher values at higher current densities. This trend is due to the direct effect of increasing current density on the overpotentials, as in Eqs. (20), 22. According to these equations, by increasing the cell's temperature, the overpotentials will decrease, which causes a decrease in cell potential and an increase in efficiency. For example, when temperature increases from 40 °C to 80 °C at i = 4400 A/m$^2$, electrolyzer efficiency experiences a rise of 2.6%.

#### 4.2.4. Methanol synthesis unit

Figs. 15-17 depict the variations of methanol concentration, $CO_2$ conversion, and temperature profiles along the reactor axial distance at five different inlet temperatures. At first, carbon dioxide is converted to methanol through a hydrogenation reaction and to carbon monoxide through a reverse water–gas shifting reaction. These reactions lead to an increase in methanol concentration and carbon dioxide conversion, as shown in Fig. 15 and Fig. 16, respectively. As mentioned in Eqs. 27–29, hydrogenation reaction is exothermic, but reverse shifting reaction is endothermic. Since hydrogenation reaction rate is more than the RWGS reaction, the overall thermal effect is the rise of reactor temperature in Fig. 17. As the stream proceeds in the reactor, the concentration of $CO_2$ decreases, and both reactions attain a thermodynamic equilibrium state at a definite distance from the reactor inlet. At this point, methanol concentration, $CO_2$ conversion, and reactor temperature are at their peak. The place and properties of the equilibrium point depend strongly on the inlet temperature. As demonstrated in Figs. 15-17, higher inlet

**Table 10**
Energy balance.

| Unit | Input energy (MW) | | | Output energy (MW) | | |
|---|---|---|---|---|---|---|
| | Electrical | Thermal | Chemical | Electrical | Thermal | Chemical |
| ORC | 0.047 | – | – | 1.132 | – | – |
| CC | 3.926 | 31.56 | – | – | – | – |
| PEME | 1320 | 7.945 | – | – | – | 985.28 |
| MSU | 37.28 | – | 173.015 | – | 6.329 | 136.33 |
| DMFC | 0.56 | 0.202 | 20.668 | 1.819 | – | – |

**Table 11**
Stream's conditions.

| St. No. | 1 | 2 | 3 | 4 | 5 | 6 | 7 | 8 | 9 |
|---|---|---|---|---|---|---|---|---|---|
| m (t/h) | 170 | 20.45 | 190.45 | 190.45 | 72.85 | 72.85 | 72.85 | 72.85 | 72.85 |
| T (C) | 220 | 220 | 220 | 50 | 110 | 67.67 | 30 | 30 | 30.73 |
| P (bar) | 0.95 | 0.95 | 0.95 | 0.75 | 14 | 3.2 | 3 | 3 | 14.2 |
| **St. No.** | **10** | **11** | **12** | **13** | **14** | **15** | **16** | **17** | **18** |
| m (t/h) | 190.45 | 190.45 | 190 | 0.45 | 0.45 | 472.5 | 179.3 | 483.2 | 483.2 |
| T (C) | 119.2 | 45 | 45 | 45 | 45.01 | 45 | 65.46 | 49.93 | 49.96 |
| P (bar) | 1.4 | 1.2 | 1.2 | 1.2 | 3 | 1.4 | 1 | 1.1 | 2.5 |
| **St. No.** | **19** | **20** | **21** | **22** | **23** | **24** | **25** | **26** | **27** |
| m (t/h) | 483.2 | 30.41 | 452.8 | 452.8 | 452.8 | 19.67 | 0.03 | 472.5 | 472.5 |
| T (C) | 105 | 35.17 | 120.5 | 120.6 | 57.65 | 57.65 | 57.65 | 60.01 | 45 |
| P (bar) | 2 | 1.7 | 1.9 | 2.4 | 1.9 | 1.9 | 1.9 | 1.9 | 1.4 |
| **St. No.** | **28** | **29** | **30** | **31** | **32** | **33** | **34** | **35** | **36** |
| m (t/h) | 210.4 | 223.4 | 223.4 | 223.4 | 223.4 | 279.2 | 279.2 | 0 | 25 |
| T (C) | 25 | 29.37 | 45.88 | 50.46 | 80 | 80 | 80 | 80 | 80 |
| P (bar) | 3 | 3 | 2.5 | 2 | 1.5 | 1.5 | 1.5 | 1.5 | 1.5 |
| **St. No.** | **37** | **38** | **39** | **40** | **41** | **42** | **43** | **44** | **45** |
| m (t/h) | 254.2 | 198.4 | 55.8 | 55.8 | 55.8 | 25 | 198.4 | 32.53 | 32.53 |
| T (C) | 80 | 80 | 80 | 80 | 80.01 | 35 | 55.88 | 34.79 | 133.7 |
| P (bar) | 1.5 | 1.5 | 1.5 | 1.5 | 1.55 | 1 | 1 | 1.013 | 3.2 |
| **St. No.** | **46** | **47** | **48** | **49** | **50** | **51** | **52** | **53** | **54** |
| m (t/h) | 32.53 | 32.26 | 0.27 | 32.26 | 32.26 | 32.07 | 0.19 | 32.07 | 32.07 |
| T (C) | 35 | 35 | 35 | 134.4 | 35 | 35 | 35 | 136.3 | 35 |
| P (bar) | 2.7 | 2.7 | 2.7 | 8.54 | 8.04 | 8.04 | 8.04 | 25.4 | 24.9 |
| **St. No.** | **55** | **56** | **57** | **58** | **59** | **60** | **61** | **62** | **63** |
| m (t/h) | 32.01 | 0.06 | 32.01 | 0.52 | 25 | 25 | 25 | 25 | 20.61 |
| T (C) | 35 | 35 | 140.5 | 35 | 179.4 | 35 | 179.5 | 35 | 35 |
| P (bar) | 24.9 | 24.9 | 78 | 2.7 | 3.17 | 2.67 | 8.46 | 7.96 | 7.96 |
| **St. No.** | **64** | **65** | **66** | **67** | **68** | **69** | **70** | **71** | **72** |
| m (t/h) | 4.39 | 4.39 | 4.39 | 4.39 | 36.4 | 170.4 | 170.4 | 170.4 | 93.71 |
| T (C) | 35 | 179.6 | 35 | 179.2 | 156.5 | 61.03 | 210 | 287.9 | 287.9 |
| P (bar) | 7.96 | 25.25 | 24.75 | 78 | 78 | 78 | 77.5 | 76.47 | 76.47 |
| **St. No.** | **73** | **74** | **75** | **76** | **77** | **78** | **79** | **80** | **81** |
| m (t/h) | 76.69 | 93.71 | 170.4 | 170.4 | 135.9 | 34.5 | 134.5 | 134.5 | 134.5 |
| T (C) | 287.9 | 82.62 | 83.25 | 35 | 35 | 35 | 35 | 39.7 | 39.7 |
| P (bar) | 76.47 | 74.97 | 74.97 | 74.47 | 74.47 | 74.47 | 74.47 | 78 | 78 |
| **St. No.** | **82** | **83** | **84** | **85** | **86** | **87** | **88** | **89** | **90** |
| m (t/h) | 34.5 | 34.5 | 34.18 | 34.18 | 21.66 | 12.52 | 76.69 | 76.69 | 21.66 |
| T (C) | 35.26 | 34.66 | 34.66 | 80 | 64.13 | 101.8 | 151.5 | 84.08 | 77.2 |
| P (bar) | 12 | 1.6 | 1.6 | 1.1 | 1 | 1.08 | 75.97 | 75.47 | 1.2 |
| **St. No.** | **91** | **92** | **93** | **94** | **95** | **96** | **97** | **98** | **99** |
| m (t/h) | 21.66 | 21.64 | 18.36 | 3.28 | 12.52 | 12.52 | 1.74 | 18.71 | 18.71 |
| T (C) | 35 | 35 | 35 | 35 | 101.8 | 101.8 | 30.51 | 25 | 33.31 |
| P (bar) | 1 | 1 | 1 | 1 | 3 | 3 | 1 | 1.013 | 1.1 |
| **St. No.** | **100** | **101** | **102** | **103** | **104** | **105** | **106** | **107** | **108** |
| m (t/h) | 20.45 | 0 | 20.45 | 20.45 | 8.55 | 8.55 | 8.55 | 3.18 | 53.94 |
| T (C) | 1250 | 1250 | 1250 | 220 | 120 | 120.5 | 380 | 25 | 47.57 |
| P (bar) | 1 | 1 | 1 | 0.95 | 2 | 43 | 42 | 2 | 1 |
| **St. No.** | **109** | **110** | **111** | **112** | **113** | **114** | **115** | **116** | **117** |
| m (t/h) | 53.94 | 53.94 | 86.55 | 86.55 | 86.55 | 95.33 | 45.16 | 140.5 | 101.8 |
| T (C) | 47.58 | 50 | 25 | 48.01 | 50 | 50 | 50 | 50 | 50 |
| P (bar) | 1.313 | 1.013 | 1.013 | 1.267 | 1.013 | 1.013 | 1.013 | 1.013 | 1.013 |
| **St. No.** | **118** | **119** | **120** | **121** | **122** | **123** | **124** | **125** | **126** |
| m (t/h) | 38.74 | 91.46 | 10.29 | 101.8 | 91.46 | 10.29 | 2.13 | 36.61 | 10.29 |
| T (C) | 50 | 50 | 50 | 50 | 50 | 50 | 50 | 50 | 50 |
| P (bar) | 1.013 | 1.013 | 1.013 | 1.013 | 1.013 | 1.013 | 1.013 | 1.013 | 1.013 |
| **St. No.** | **127** | **128** | | | **Purge1** | **Purge2** | **Purge3** | **Purge4** | **Purge5** |
| m (t/h) | 36.61 | 2.13 | | | 0 | 1.4 | 0.32 | 0.02 | 0 |
| T (C) | 50 | 50 | | | 60.01 | 35 | 34.66 | 35 | 47.57 |
| P (bar) | 1.013 | 1.013 | | | 1.9 | 74.47 | 1.6 | 1 | 1 |

**Table 12**
Performance parameters of the subsystems and overall system.

| Parameter | Value |
|---|---|
| **ORC** | |
| $W_{net,ORC}$ (kW) | 1085 |
| $\eta_{ORC}$ (%) | 11.15 |
| **CC** | |
| $CO_2$ recovery (%) | 90.74 |
| Reboiler duty (GJ/$t_{CO2}$) | 3.79 |
| Lean loading (mol $CO_2$/mol MEA) | 0.203 |
| Rich loading (mol $CO_2$/mol MEA) | 0.496 |
| $pH_{lean}$ | 9.79 |
| $pH_{rich}$ | 8.52 |
| **PEME** | |
| Current density (A/$m^2$) | 7186 |
| Voltage (V) | 1.986 |
| Power (MW) | 1320 |
| $\eta_{PEME}$ (%) | 74.20 |
| **MSU** | |
| $CO_2$ conversion in the reactor (%) | 21.30 |
| $CO_2$ conversion in the unit (%) | 94.84 |
| Methanol selectivity (%) | 97.70 |
| Methanol yield (%) | 20.81 |
| Methanol production (t/d) | 518.88 |
| **DMFC** | |
| Current density (A/$m^2$) | 2082 |
| Voltage (V) | 0.25 |
| Power (MW) | 1.82 |
| $\eta_{cell}$ (%) | 8.83 |
| $\eta_{DMFC}$ (%) | 8.49 |
| Overall energy efficiency (%) | 66.84 |
| Overall exergy efficiency (%) | 55.10 |

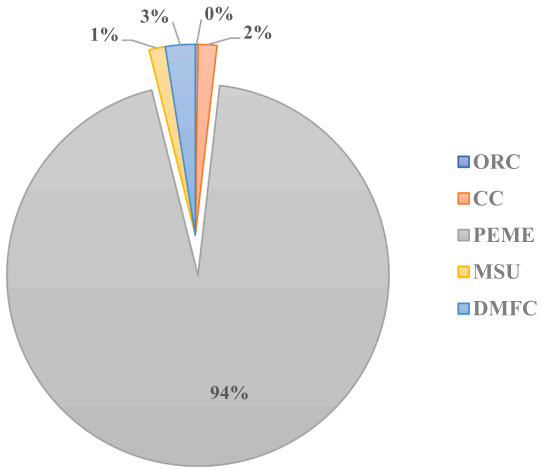


**Fig. 8.** Portion of each subsystem in total exergy destruction.

temperature leads to the earlier establishment of equilibrium condition, so the equilibrium distance from the reactor inlet decreases. The reason is that high inlet temperature improves the kinetic rate of both reactions. At an inlet temperature of 200 °C, the reactions are kinetically so limited and slow that no equilibrium state is achieved inside the reactor. At the inlet temperature of 210 °C, both reactions occur at a high rate, and hence, maximum equilibrium methanol concentration and $CO_2$ conversion are gained. If the reactor inlet temperature is more than 210 °C, RWGS attains its equilibrium earlier and then proceeds in the reverse direction, resulting in the lower equilibrium methanol concentration and $CO_2$ conversion. In other words, the exothermic nature of $CO_2$ hydrogenation prefers low inlet temperature. On the other hand, very low temperature slows down the kinetic rates of the reactions. So, there is an optimum inlet temperature that can satisfy these two contradictory issues, and it is 210 °C in this case. Furthermore, the higher the inlet temperature, the higher the reactor temperature, as in Fig. 17.

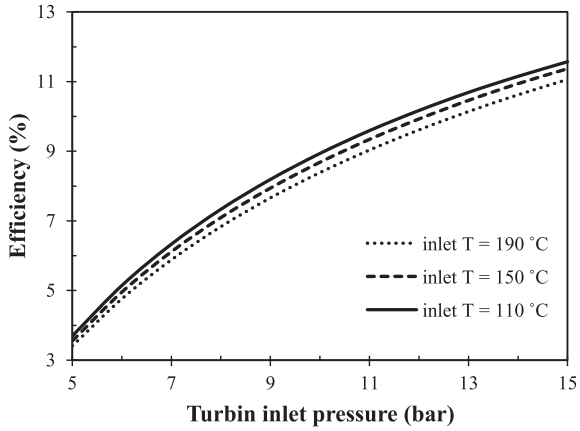


**Fig. 9.** Effect of turbine inlet pressure on ORC efficiency at different values of turbine inlet temperature.

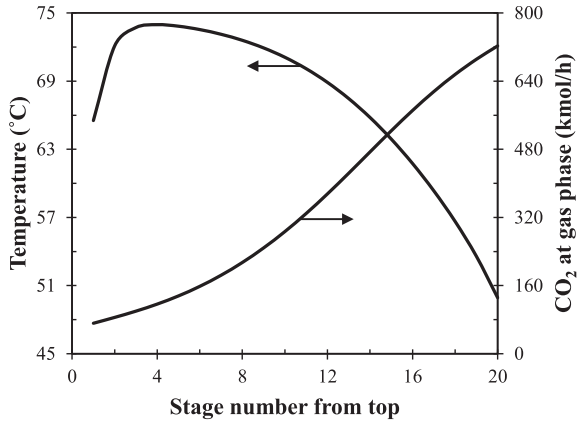


**Fig. 10.** Profiles of temperature and gas-phase $CO_2$ molar flowrate inside the absorber column.

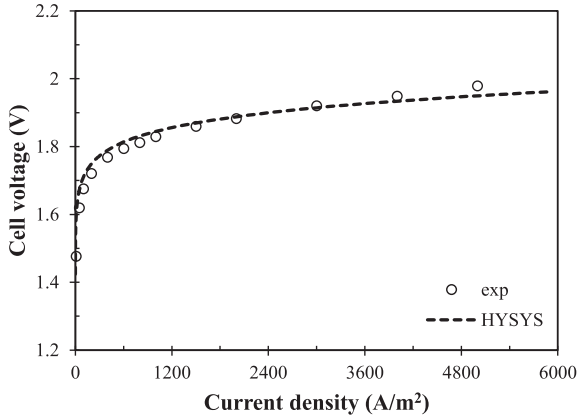


**Fig. 11.** Simulation results of PEME from present work versus experimental data.

In Fig. 18, the effect of inlet temperature and pressure on carbon dioxide conversion is plotted. According to Fig. 15-Fig. 17, at 200 °C, the reactions inside the reactor did not reach an equilibrium state. Therefore, with increasing temperature, the rate of reactions is increased, leading to an increase in the $CO_2$ conversion. Also, according to these figures, at 210 °C and above, the reactions reach equilibrium. So, in these conditions, Le Chatelier's principle can be applied. Since the overall reaction of methanol synthesis is exothermic, the conversion of

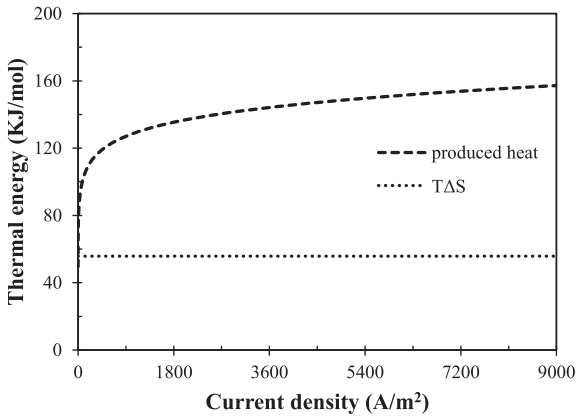


**Fig. 12.** Comparison between heat demand and produced heat of PEME at 80 °C.

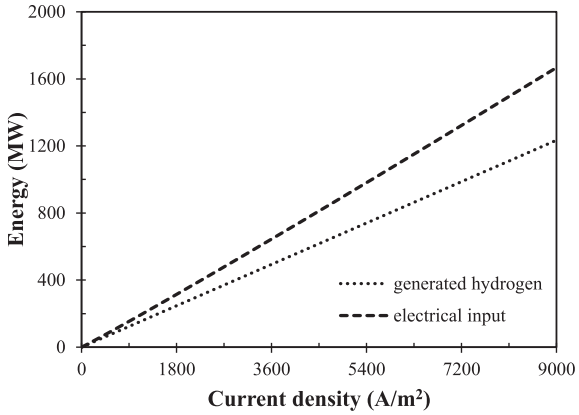


**Fig. 13.** Effect of electrolyzer current density on electrical input power and generated hydrogen energy at 80 °C.

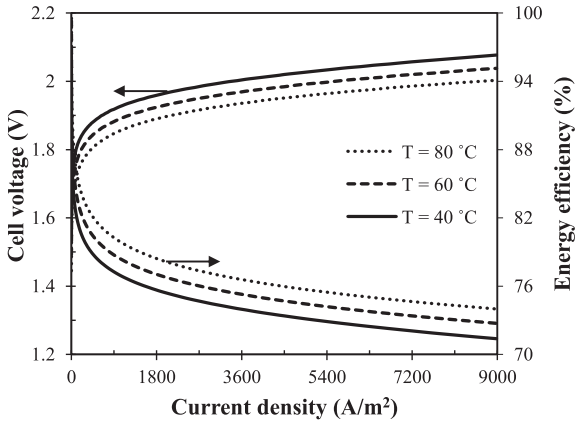


**Fig. 14.** Effect of temperature on electrolyzer voltage and energy efficiency.

$CO_2$ decreases with increasing temperature. As a result, when the temperature rises from 200 °C to 275 °C at constant pressure, $CO_2$ conversion first increases to a maximum value, then decreases linearly. The value of maximum $CO_2$ conversion depends on the reactor inlet pressure, but it always occurs at a temperature of about 210 °C. Also, Fig. 18 demonstrates that the effect of changing inlet pressure on the $CO_2$ conversion is related to the reactor inlet temperature. In other words, if the reactor inlet temperature is less than 210 °C (temperature of the maximum point), $CO_2$ conversion worsens as inlet pressure rises.

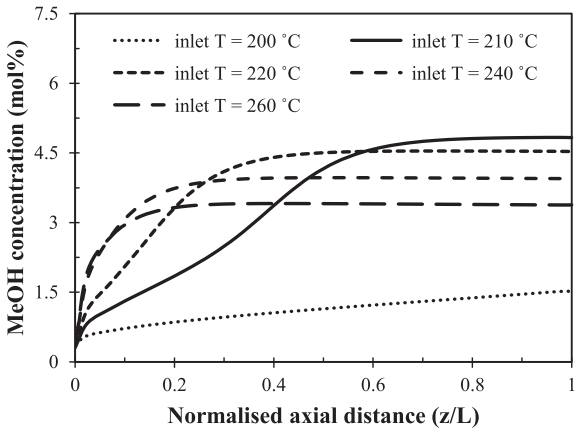


**Fig. 15.** Effect of reactor inlet temperature on the methanol concentration profile at 75 bar.

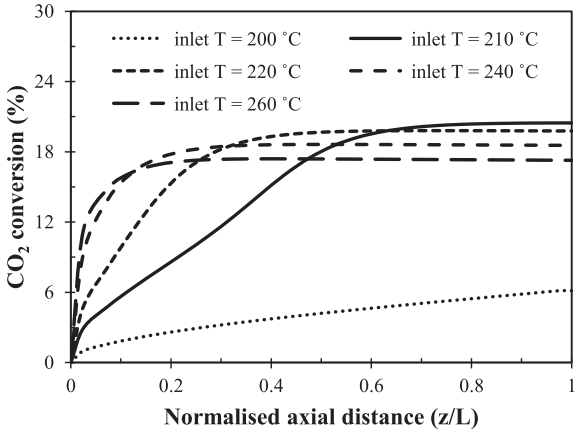


**Fig. 16.** Effect of reactor inlet temperature on $CO_2$ conversion profile at 75 bar.

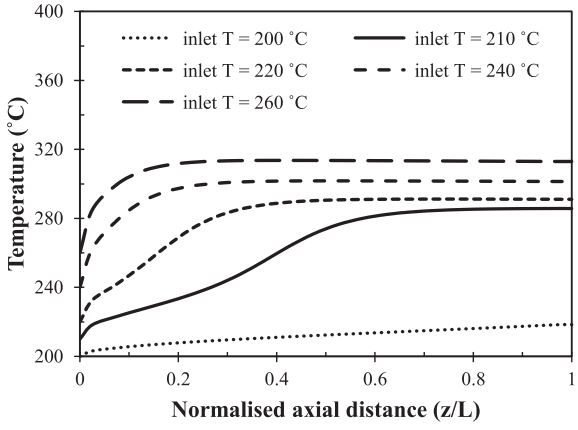


**Fig. 17.** Effect of reactor inlet temperature on temperature profile at 75 bar.

However, when the inlet temperature is more than 210 °C, $CO_2$ conversion and inlet pressure directly relate. As inlet pressure increases, hydrogenation reactions (Eq. (27), 28) move forward according to Le Chatelier's principle. Hence more amount of methanol is produced, and $CO_2$ conversion rises. Moreover, the dependence of $CO_2$ conversion on the pressure is intensified for higher temperatures. For instance, changing pressure from 50 to 80 bar at a temperature of 200 °C causes a 1.583% decrease in $CO_2$ conversion, while, at 250 °C, the increase of $CO_2$ conversion is 5.097%.

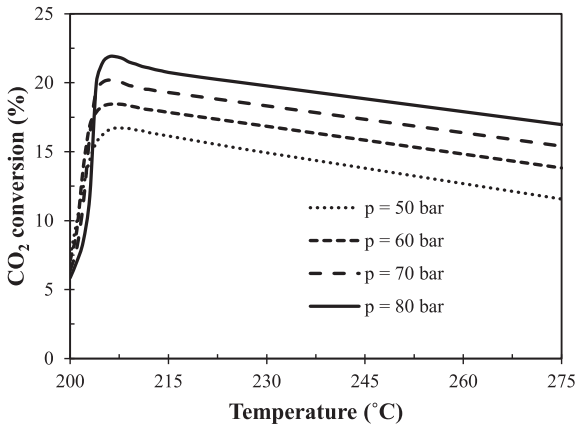


**Fig. 18.** Effect of reactor inlet temperature and pressure on $CO_2$ conversion.

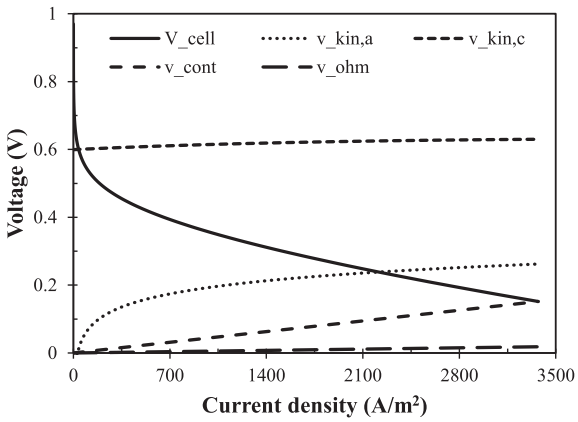


**Fig. 20.** Effect of DMFC current density on cell voltage and overpotentials.

#### 4.2.5. *Direct methanol fuel cell*

The obtained results for the DMFC are compared with the experimental data in [48] in the form of a cell voltage-current density plot at the same operating conditions to validate the simulation of the DMFC in this work. As shown in Fig. 19, there is a good agreement between them, and the developed model can predict the behavior of DMFC very well. The deviation at low values of current density is due to the kinetic expressions of MOR and ORR, Eqs. (54) and (55), and their parameters, Eq. (56). On the other hand, deviation at high current density is attributed to limited reaction rates and liquid fuel diffusion rate, beside the ignorance of two-phase effects in the simulation code.

The effect of changing DMFC current density on its overpotentials and cell voltage is shown in Fig. 20. The calculation reveals that the thermodynamic equilibrium voltage is 1.214 v, which is much higher than the open-circuit voltage, i.e., cell voltage at zero current density. The reason is the methanol crossover phenomenon in the fuel cell and significant cathode overpotential even when no current is applied. Other overpotentials are zero when there is no current density. As DMFC current density rises, cathode overpotential has an approximately constant trend because of two conflicting factors: methanol crossover and real performance of DMFC. According to Fig. 20, other overpotentials start to increase with the current density. This procedure is expectable if Eqs. (22), 57, 58, and 60 are considered. The rate of anode overpotential increase is high, but the amount of membrane ohmic overpotential is little at all current densities. Finally, the increase of overpotentials with current density leads to a decrease in cell voltage.

The curves of efficiencies and power density of DMFC against current density is depicted in Fig. 21. By increasing the utilization of methanol in the cell, the voltage efficiency decreases (Eq. (63)) while the fuel efficiency increases (Eq. (64)). At low current densities, fuel efficiency is a dominant factor in cell efficiency, while at high current densities, the voltage efficiency is prominent. Consequently, the cell efficiency curve has a maximum value, as shown in Fig. 21. Also, as current density rises, DMFC power density first increases to its maximum value, then it decreases. Eq. (52) shows that fuel cell power density is dependent on two contradictory parameters: current density and cell voltage. At low current density, the effect of increasing DMCF current density is prominent, while at high current density, the decreasing rate of cell voltage is determinant for power density.

Fig. 22 displays changes in cell voltage and power density with current density at different operating temperatures. This figure demonstrates that a rise in fuel cell operating temperature enhances its voltage and power density since higher temperature improves the reactants transport properties and the kinetics of the electrochemical reaction. However, the operating temperature has an adverse effect on the limiting current density because of the increasing rate of methanol crossover.

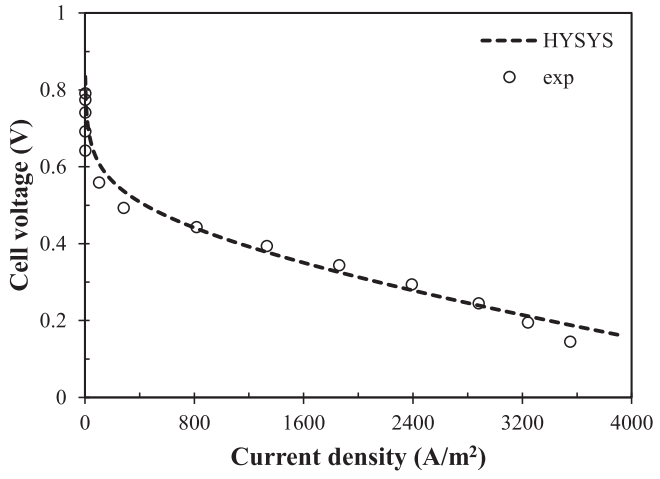


**Fig. 19.** Comparison between simulation results of DMFC with Aspen HYSYS and experimental data.

## 5. Conclusions

A novel trigeneration system including organic Rankine cycle (ORC), carbon capture unit (CC), proton exchange membrane electrolyzer (PEME), methanol synthesis unit (MSU), and direct methanol fuel cell (DMFC) is proposed and analyzed from a thermodynamic viewpoint in this paper. The proposed system decreases the carbon emission rate, captures most part of flue gas carbon dioxide, and generates methanol, hydrogen, and power. The ORC system justifies the temperature of flue

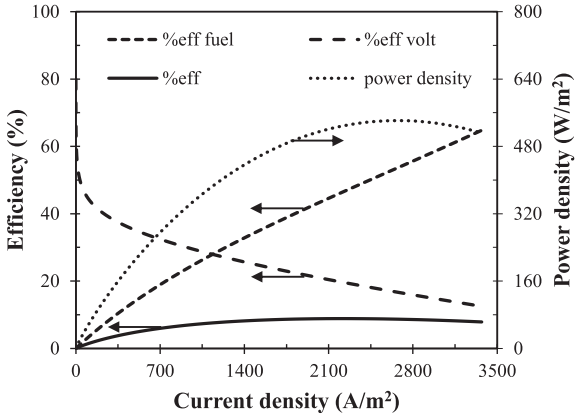


**Fig. 21.** Effect of DMFC current density on efficiencies and power density.

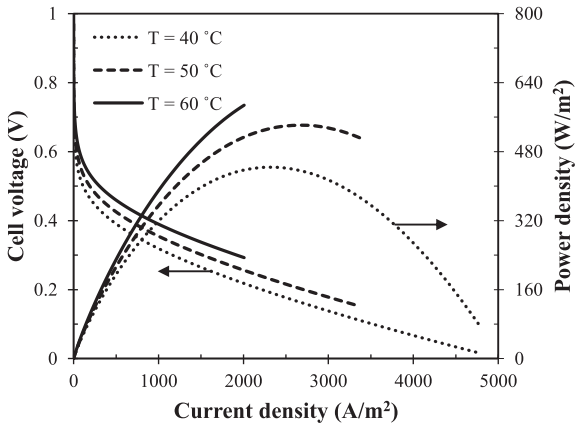


**Fig. 22.** Effect of DMFC current density and operating temperature on cell voltage and power density.

gas for the carbon capture process. A solar system is used to provide the power demand of PEME. Part of the generated hydrogen is sent to the methanol synthesis unit for carbon hydrogenation reaction, and the rest is stored for utilization in night/cloudy times or sales. The main results of the present work can be concluded as follows:

- PEME system has the highest contribution to the overall exergy destruction rate because of its considerable power consumption, electrochemical reactions, and thermal interactions. On the other hand, ORC has a negligible effect on total exergy destruction since no reaction occurs in this cycle.
- The energy and exergy efficiencies of the system are calculated as 66.84% and 55.10%, respectively.
- Increasing ORC turbine inlet pressure enhances ORC system efficiency, while an increase in its turbine inlet temperature deteriorates the ORC efficiency.
- The carbon capture rate is high at the bottom stages of the CC absorber column. Then, it gets slower. Also, as the stream moves in the absorber column, temperature attains its maximum value at the fourth stage.
- As the current density of PEME increases, its cell voltage increases, but PEME energy efficiency decreases.
- Reactor inlet temperature has a crucial effect on methanol concentration, $CO_2$ conversion, and temperature profiles along the reactor length. Even the impact of reactor inlet pressure on carbon conversion depends on its inlet temperature.
- As the current density of DMFC rises, cell efficiency and power density increase to their maximum values, then decrease.
- Although the higher operating temperature of DMFC has a positive effect on cell voltage and power density, it limits the fuel cell current density.

## CRediT authorship contribution statement

**Reza Nazerifard:** Conceptualization, Writing - original draft, Investigation. **Leyla Khani:** Writing - original draft, Validation. **Mousa Mohammadpourfard:** Conceptualization, Supervision. **Behnam Mohammadi-Ivatloo:** Writing - review & editing. **Gülden Gökcen Akkurt:** Writing - review & editing.

## Declaration of Competing Interest

The authors declare that they have no known competing financial interests or personal relationships that could have appeared to influence the work reported in this paper.

## References

[1] Choi W-J, Seo J-B, Jang S-Y, Jung J-H, Oh K-J. Removal characteristics of $CO_2$ using aqueous MEA/AMP solutions in the absorption and regeneration process. J Environ Sci 2009;21:907–13.
[2] Bryant S. Geologic $CO_2$ storage—can the oil and gas industry help save the planet? J Petrol Technol 2007;59:98–105.
[3] Ribeiro AM, Santos JC, Rodrigues AE. PSA design for stoichiometric adjustment of bio-syngas for methanol production and co-capture of carbon dioxide. Chem Eng J 2010;163:355–63.
[4] Peters M, Köhler B, Kuckshinrichs W, Leitner W, Markewitz P, Müller TE. Chemical technologies for exploiting and recycling carbon dioxide into the value chain. ChemSusChem 2011;4:1216–40.
[5] Quadrelli EA, Centi G, Duplan JL, Perathoner S. Carbon dioxide recycling: emerging large-scale technologies with industrial potential. ChemSusChem 2011;4:1194–215.
[6] Olajire AA. Valorization of greenhouse carbon dioxide emissions into value-added products by catalytic processes. Journal of $CO_2$ Utilization. 2013;3:74–92.
[7] Riaz A, Zahedi G, Klemeš JJ. A review of cleaner production methods for the manufacture of methanol. J Cleaner Prod 2013;57:19–37.
[8] Dincer I, Rosen MA, Ahmadi P. Modeling and Optimization of Multigeneration Energy Systems. Chichester, UK: Optimization of Energy Systems. John Wiley & Sons Ltd; 2017. p. 398–446.
[9] Mignard D, Sahibzada M, Duthie J, Whittington H. Methanol synthesis from flue-gas $CO_2$ and renewable electricity: a feasibility study. Int J Hydrogen Energy 2003;28:455–64.
[10] Boretti A. Renewable hydrogen to recycle $CO_2$ to methanol. Int J Hydrogen Energy 2013;38:1806–12.
[11] Sayah AK, Sayah AK. Wind-hydrogen utilization for methanol production: An economy assessment in Iran. Renew Sustain Energy Rev 2011;15(8):3570–4.
[12] Esmaili P, Dincer I, Naterer G. Development and analysis of an integrated photovoltaic system for hydrogen and methanol production. Int J Hydrogen Energy 2015;40:11140–53.
[13] Leonzio G, Zondervan E, Foscolo PU. Methanol production by $CO_2$ hydrogenation: analysis and simulation of reactor performance. Int J Hydrogen Energy 2019;44:7915–33.
[14] Atsonios K, Panopoulos KD, Kakaras E. Investigation of technical and economic aspects for methanol production through $CO_2$ hydrogenation. Int J Hydrogen Energy 2016;41:2202–14.
[15] Rivarolo M, Bellotti D, Magistri L, Massardo A. Feasibility study of methanol production from different renewable sources and thermo-economic analysis. Int J Hydrogen Energy 2016;41:2105–16.
[16] Nami H, Ranjbar F, Yari M. Methanol synthesis from renewable $H_2$ and captured $CO_2$ from S-Graz cycle–Energy, exergy, exergoeconomic and exergoenvironmental (4E) analysis. Int J Hydrogen Energy 2019;44:26128–47.
[17] Kiatphuengporn S, Donphai W, Jantaratana P, Yigit N, Föttinger K, Rupprechter G, et al. Cleaner production of methanol from carbon dioxide over copper and iron supported MCM-41 catalysts using innovative integrated magnetic field-packed bed reactor. J Cleaner Prod 2017;142:1222–33.
[18] Luu MT, Milani D, Abbas A. Analysis of $CO_2$ utilization for methanol synthesis integrated with enhanced gas recovery. J Cleaner Prod 2016;112:3540–54.
[19] Charoensuppanimit P, Kitsahawong K, Kim-Lohsoontorn P, Assabumrungrat S. Incorporation of hydrogen by-product from $NaOCH_3$ production for methanol synthesis via $CO_2$ hydrogenation: Process analysis and economic evaluation. J Cleaner Prod 2019;212:893–909.
[20] Ghosh S, Uday V, Giri A, Srinivas S. Biogas to methanol: A comparison of conversion processes involving direct carbon dioxide hydrogenation and via reverse water gas shift reaction. J Cleaner Prod 2019;217:615–26.
[21] Gao R, Zhang C, Lee Y-J, Kwak G, Jun K-W, Kim SK, et al. Sustainable production of methanol using landfill gas via carbon dioxide reforming and hydrogenation: Process development and techno-economic analysis. J Cleaner Prod 2020;272:122552. https://doi.org/10.1016/j.jclepro.2020.122552.
[22] Alsayegh S, Johnson JR, Ohs B, Wessling M. Methanol production via direct carbon dioxide hydrogenation using hydrogen from photocatalytic water splitting: Process development and techno-economic analysis. J Cleaner Prod 2019;208:1446–58.
[23] Matzen M, Demirel Y. Methanol and dimethyl ether from renewable hydrogen and carbon dioxide: Alternative fuels production and life-cycle assessment. J Cleaner Prod 2016;139:1068–77.
[24] Abam FI, Briggs TA, Ekwe EB, Kanu CG, Effiom SO, Ndukwu MC, et al. Exergy analysis of a novel low-heat recovery organic Rankine cycle (ORC) for combined cooling and power generation. Energy Sources Part A 2019;41(13):1649–62.
[25] Zhou N, Wang X, Chen Z, Wang Z. Experimental study on Organic Rankine Cycle for waste heat recovery from low-temperature flue gas. Energy. 2013;55:216–25.
[26] Guo C, Du X, Yang L, Yang Y. Organic Rankine cycle for power recovery of exhaust flue gas. Appl Therm Eng 2015;75:135–44.
[27] Laribi S, Dubois L, De Weireld G, Thomas D. Study of the post-combustion $CO_2$ capture process by absorption-regeneration using amine solvents applied to cement plant flue gases with high $CO_2$ contents. Int J Greenhouse Gas Control 2019;90:102799.
[28] G. Léonard. Optimal design of a CO2 capture unit with assessment of solvent degradation. Université de Liège, Liège, Belgique2013.
[29] Ursua A, Gandia LM, Sanchis P. Hydrogen production from water electrolysis: current status and future trends. Proc IEEE 2011;100:410–26.
[30] Millet P, Mbemba N, Grigoriev S, Fateev V, Aukauloo A, Etiévant C. Electrochemical performances of PEM water electrolysis cells and perspectives. Int J Hydrogen Energy 2011;36:4134–42.

[31] Jamali Ghahderijani M, Ommi F. One-dimensional electrolyzer modeling and system sizing for solar hydrogen production: an economic approach. J Renew Energy Environ 2016;3:31–43.
[32] García-Valverde R, Espinosa N, Urbina A. Simple PEM water electrolyser model and experimental validation. Int J Hydrogen Energy 2012;37:1927–38.
[33] Awasthi A, Scott K, Basu S. Dynamic modeling and simulation of a proton exchange membrane electrolyzer for hydrogen production. Int J Hydrogen Energy 2011;36:14779–86.
[34] Ni M, Leung MK, Leung DY. Energy and exergy analysis of hydrogen production by a proton exchange membrane (PEM) electrolyzer plant. Energy Convers Manage 2008;49:2748–56.
[35] Ruuskanen V, Koponen J, Huoman K, Kosonen A, Niemelä M, Ahola J. PEM water electrolyzer model for a power-hardware-in-loop simulator. Int J Hydrogen Energy 2017;42:10775–84.
[36] Anicic B, Trop P, Goricanec D. Comparison between two methods of methanol production from carbon dioxide. Energy 2014;77:279–89.
[37] Van-Dal ÉS, Bouallou C. Design and simulation of a methanol production plant from CO2 hydrogenation. J Cleaner Prod 2013;57:38–45.
[38] Ko J, Chippar P, Ju H. A one-dimensional, two-phase model for direct methanol fuel cells–Part I: Model development and parametric study. Energy 2010;35:2149–59.
[39] Yin K-M. A theoretical model of the membrane electrode assembly of liquid feed direct methanol fuel cell with consideration of water and methanol crossover. J Power Sources 2008;179:700–10.
[40] Sharifi S, Rahimi R, Mohebbi-Kalhori D, Colpan CO. Numerical investigation of methanol crossover through the membrane in a direct methanol fuel cell. Iran J Hydrogen Fuel Cell 2018;5:21–33.
[41] Meyers Jeremy P, Newman John. Simulation of the direct methanol fuel cell: II. Modeling and data analysis of transport and kinetic phenomena. J Electrochem Soc 2002;149(6):A718. https://doi.org/10.1149/1.1473189.
[42] Bernardi DM, Verbrugge MW. Mathematical model of a gas diffusion electrode bonded to a polymer electrolyte. AIChE J 1991;37:1151–63.
[43] Wang ZH, Wang CY. Mathematical modeling of liquid-feed direct methanol fuel cells. J Electrochem Soc 2003;150(4):A508. https://doi.org/10.1149/1.1559061.
[44] Lee J, Lee S, Han D, Gwak G, Ju H. Numerical modeling and simulations of active direct methanol fuel cell (DMFC) systems under various ambient temperatures and operating conditions. Int J Hydrogen Energy 2017;42:1736–50.
[45] Xu C, Faghri A. Analysis of an active tubular liquid-feed direct methanol fuel cell. J Power Sources 2011;196:6332–46.
[46] Kvamsdal HM, Rochelle GT. Effects of the temperature bulge in $CO_2$ absorption from flue gas by aqueous monoethanolamine. Ind Eng Chem Res 2008;47:867–75.
[47] Ioroi T, Yasuda K, Siroma Z, Fujiwara N, Miyazaki Y. Thin film electrocatalyst layer for unitized regenerative polymer electrolyte fuel cells. J Power Sources 2002;112:583–7.
[48] Ge J, Liu H. Experimental studies of a direct methanol fuel cell. J Power Sources 2005;142:56–69.